NTNU
Norwegian University of
Science and Technology

Vapour Pressure of Bi above Bi-Ti Alloys by Transpiration Method

Nina Lu Thomassen

Chemical Engineering and Biotechnology
Submission date: July 2017
Supervisor: Geir Martin Haarberg, IMA
Co-supervisor: Tetsuya Uda, Kyoto University

Norwegian University of Science and Technology
Department of Materials Science and Engineering

Preface

The work presented in this thesis was carried out as part of an exchange program at the Department of Material Science and Engineering at Kyoto University, Japan. The thesis is written as part of the Master program Chemical Engineering and Biotechnology at the Norwegian University of Science and Technology (NTNU). Professor Tetsuya Uda of Kyoto University and Professor Geir Martin Haarberg of NTNU have given joint supervision. This work is a continuation of research on developing a new titanium production process in Professor Uda's laboratory group, and was carried out between January and July 2017.

I wish to thank both my supervisors for all their help and support during this work. I also thank Professor Geir Martin Haarberg for making this exchange possible, and Professor Tetsuya Uda for accepting me into his group and taking me under his supervision. The feedback and guidance during the final stage of my education are greatly appreciated. Additonally, I would like to give a special thanks to Professor Haarberg, who stayed in Japan during my first three months, for taking me sightseeing and teaching me about Japanese culture. I also owe a great thanks to Kyoto International Forum for Environment and Energy (KIFEE) for giving me a mobility grant during my stay in Japan. Finally, I would like to express my deepest gratitude to PhD student Akihiro Kishimoto for all the help he has given me, both with the experimental work and the discussions and explanations during this work. I am so grateful that whenever I needed help he took the time to help me, whether it was with the laboratory work, my understanding of thermodynamics or discussion of my results.

Abstract

Titanium is an attractive metal with wide-ranging applications due to its properties. Titanium is one of the most corrosion resistant metals with the highest strength-to-weight ratio. The only industrial production route for titanium today is by the Kroll process, which involves a magnesiothermic reduction of $TiCl_4$. However, this process is slow and inefficient, and a new production route for titanium is therefore desirable. Recently, a more efficient alternative production route was proposed by Kado *et al.* [1], involving magnesiothermic reduction of $TiCl_2$ into a liquid Bi cathode. However, to determine the feasibility of this new method, a better understanding of the underlying operating conditions is still required. In this work, the thermodynamic properties of the Bi−Ti system are therefore experimentally investigated. Specifically, various vapour pressure measurements were carried out to determine the vapour pressure of Bi above various samples by the transpiration method. The samples were pure Bi, Bi−30 mol% Ti alloy, Bi−40 mol% Ti alloy, Bi−50 mol% Sn alloy, and Bi−70 mol% Sn alloy at 900°C. Additionally, a few experiments were conducted with pure Bi at 800°C. Using previous literature, the expected value for the vapour pressure of Bi over Bi−Ti alloys were calculated and compared to the empirical values, but no agreement was observed as the empirical values were too high. Therefore, measurements with Bi−Sn alloys were performed in order to verify that the experimental equipment was operating correctly. The literature value for the vapour pressure of Bi above Bi−Sn alloys was also calculated and compared with the measured values, and determined to be in great agreement, indicating that the experimental equipment was operating as predicted.

Sammendrag

Titan er et attraktivt metall med et bredt applikasjonsområde på grunn av dens egenskaper. For eksempel er titan et av de mest korrosjonsbestandige metaller med høyest stryke i forhold til vekt. Den eneste industrielle produksjonsruten for titan i dag er ved Krollprosessen, som innebærer en magnesiotermisk reduksjon av $TiCl_4$. Denne prosessen er imidlertidig langsom og ineffektiv, og derfor er en ny produksjonsprosess ønskelig. En ny og mer effektiv alternativ produksjonsmetode ble nylig foreslått av Kado *m.fl.* [1], som innvolverer magnesiotermisk reduksjon av $TiCl_2$ i en flytende Bi-katode. For å fastslå muligheten for denne nye metoden er det imidlertid nødvendig med en bedre forståelse av driftsforholdene. I dette arbeidet blir de termodynamiske egenskapene til Bi – Ti systemet undersøkt eksperimentelt. Forskjellige fordampningstrykkmålinger for å bestemme fordampningstrykket til Bi over forskjellige prøver ble utført ved transpirasjonsmetoden. Eksperimenter ble utført med prøvene: ren Bi, Bi – 30 % Ti legering, Bi – 40 mol% Ti legering, Bi – 50 mol% Sn legering og Bi – 70 mol% Sn legering ved 900°C. I tillegg ble eksperimenter med ren Bi ved 800°C utført. Den forventede verdien for damptrykket av Bi over Bi – Ti-legeringene ble beregnet med hensyn til tidligere litteraturverdier, og sammenlignet med de empiriske verdiene. De empiriske verdiene oppnådd, hadde høyere verdi enn de utregnede fra litteraturverdiene, og ingen overensstemmelse ble observert. Derfor ble det utført eksperimenter med Bi – Sn-legeringer for å verifisere at det eksperimentelle utstyret fungerte riktig. Litteraturverdien for damptrykket av Bi over Bi – Sn legeringer ble også beregnet og sammenlignet med de målte verdiene, og fastslått å være i god overensstemmelse. Dette indikerte at det eksperimentelle utstyr fungerte som forventet.

Contents

Chapter 1

Introduction

Titanium constitutes about 0.44% of the earth crust and is an important structural metal due to its properties, such as low density, high strength and excellent corrosion resistance [2]. Titanium became more available after World War II, and it was predicted to be as commonplace as aluminium [3]. Unfortunately, the high price put a restriction on this, mainly due to the high cost of extraction. Although it is an electrochemically active metal, it forms a protective oxide film that makes it immune to corrosion in several harsh environments [4]. Together with excellent corrosion resistance, titanium is also the metal with the highest strength-to-weight ratio and about 60% of the density of steel with the same strength [5]. These properties can easily be modified, for example by alloying titanium with 6% aluminium and 4% vanadium, and the strength is almost doubled with a lower net weight. These properties make titanium an attractive material, and it is extensively used in the aerospace industry. For example, the use of titanium materials in commercial jet planes has been increasing, with the total airframe of Boeing 787 consisting of 14% titanium [6]. Titanium is also a biocompatible metal, meaning the human body will not reject it, nor will it corrode in body fluid [7]. It is therefore suitable for medical applications, and today it is applied to orthopaedic implants and dental use. Titanium is also non-magnetic, meaning magnetic resonance imaging (MRI) can be used safely on patients with titanium implants.

In 1937 William J. Kroll invented the Kroll process which today is the only industrial process producing titanium [8]. The Kroll process is a batch process where a titanium sponge is produced by metallothermic reduction of magnesium and is a highly energy intensive process which requires about 50 kWh/kg Ti [9]. Consequently, it has become an expensive metal compared to metals such as aluminium and steel. In 1998 the price for titanium was approximately $20/kg whereas alu-

minium and steel cost \$1.5/kg and \$0.45/kg, respectively. In 2010 the price was slightly higher at about \$22/kg Ti ingot [4]. Although the price for titanium has decreased over time, it is still expensive compared to other metals, according to MetalMiner, the average price today, for a Ti-6-4 bar is around \$12.4/kg (27 April [10]). The price is still quite high, especially compared to the price for an aluminium 3003-H14 sheet which costs \$0.71/kg (27 April [10]). In 2000 a new process for titanium production was published by Fray, Farthing and Chen, which led to an increased interest in titanium research [11]. Today this process is known as the FFC Cambridge process, and it involves electrochemical reduction directly from titanium oxide (TiO_2) to form both metal and alloys. According to some reports, this process will only consume 7 kWh/kg of produced titanium which is a significant improvement compared to the Kroll process [12]. Given the excellent properties of titanium, the development of such a new feasible process would play a significant role in the coming years.

The production rate of Ti by the Kroll process is slow and inefficient, and it is therefore desirable to develop a new production route. Kado *et al.* [1] proposed a new process of magnesiothermic reduction of $TiCl_4$, into a liquid Bi cathode forming Bi−Ti alloy which then is subsequently refined by vacuum distillation. The process is described in Section 2.2.4.1, and this thesis is an extension of this work. The purpose was to experimentally determine the thermodynamic properties of Bi−Ti alloys for estimation of the proper operating conditions of vacuum distillation, segregation, and the reaction heat by reduction of $TiCl_4$ by Mg precisely. Vapour pressure measurements of Bi above Bi−Ti alloys were carried out by the transpiration method, to determine the activity of Bi in Bi−Ti alloys.

Chapter 2

Background

In 1791 William Gregor, a British amateur geologist and clergyman produced a white metallic oxide from black magnetic sand and thereby was the first to discover titanium [13]. A few years later, in 1795, German chemist Martin Heinrich Klaproth rediscovered the same oxide and named it "titanium" after the Greek Titans. Titanium can be found in almost all rocks, but for the titanium industry, the most important minerals are ilmenite ($FeTiO_3$) and rutile (TiO_2). Titanium is difficult to work with, as it will immediately react with oxygen in the atmosphere and form titanium dioxide [4]. It is also one of the few elements that will burn in pure nitrogen gas, forming titanium nitrides. Trying to produce it in the usual manner by carbon reduction will only lead to the formation of the titanium carbide, and the metal was first isolated in 1887 [14].

2.1 Early titanium production

Lars Fredrik Nilson and Otto Pettersson managed to obtain 95% pure titanium in an airtight steel cylinder by reduction of titanium tetrachloride with sodium [14]. They were the first to successfully isolate the metal, nearly 100 years after its discovery. Later, Mattew A. Hunter was able to produce 99.9% pure titanium in 1910 [15]. He modified the method of Nilson and Pettersson, by heating the titanium tetrachloride in a steel bomb with sodium, and the main reaction is given in Equation 2.1 [16]. This process is now known as the Hunter process and was the main method for producing titanium until the invention of the more economic Kroll process.

$$\mathrm{TiCl_4(g) + 4\,Na\,(l) \longrightarrow 4\,NaCl\,(l) + Ti\,(s)} \tag{2.1}$$

2.1.1 The Kroll process

The Kroll process was invented in the late 1930s, and commercialised in the mid-1940s [3]. This process is similar to the Hunter process, which uses sodium as a reducing agent [17]. However, in the Kroll process sodium is replaced with magnesium. TiO_2 is chlorinated to the raw material of the Kroll process, $TiCl_4$, which then is reduced with magnesium to form titanium. The process can be divided into three major steps:

1. Chlorination of titanium dioxide by petroleum coke
2. Reduction of titanium chloride by magnesium
3. Regeneration of magnesium by electrolysis

Figure 2.1 shows a flow chart of the Kroll process. However, this batch process is criticised for being inefficient and demanding a lot of energy, mainly due to the highly exothermic reaction in the reduction step. This causes a slow feed rate of $TiCl_4$ and hence a slow production rate of titanium. Attempts to develop a more efficient titanium process have so far been unsuccessful, such that all industrial titanium is still produced according to the Kroll process today.

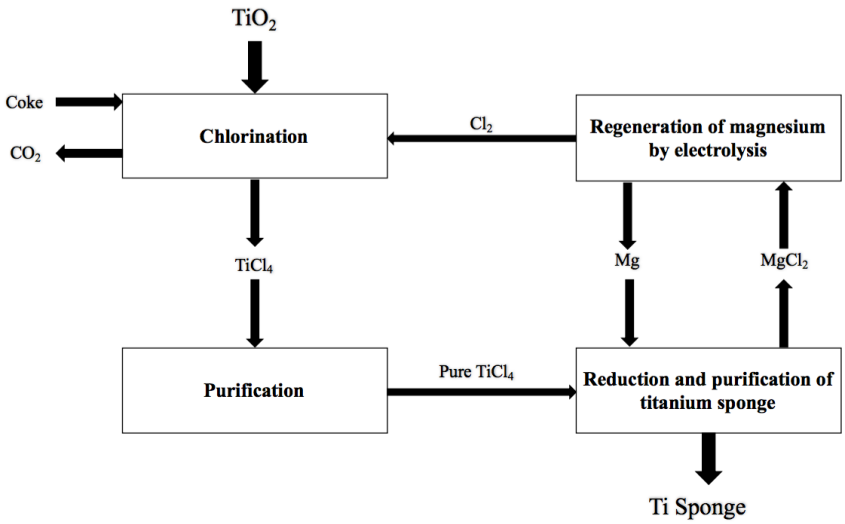

Figure 2.1: A flow chart of the Kroll process.

Chlorination step

Several minerals contain titanium, among them ilmenite ($FeTiO_3$) and rutile (TiO_2), which are the only once of economic importance [18]. Typically, natural or synthetic rutile is used in the chlorination process since ilmenite contains iron contaminations and other impurities, which requires an additional step to gain a higher content of TiO_2 [3]. The purpose of the chlorination process is to produce $TiCl_4$. To achieve this, TiO_2 is reduced with petroleum coke and chlorine gas in a fluid reactor at high temperatures (800°C-1500°C) according to Equation 2.2 [18].

$$\mathrm{TiO_2(s) + 2\,Cl_2(g) + C\,(s) \longrightarrow TiCl_4(g) + CO_2(g)} \tag{2.2}$$

Reduction step

Magnesiothermic reduction of $TiCl_4$ occurs in a dry and clean stainless steel container with argon gas in order to avoid contamination from air and moisture [3]. Magnesium is then added to the container, plus 15%-30% excess of which is needed to reduce the $TiCl_4$. The container is then heated, and $TiCl_4$ is fed slowly into the container and reduced according to Equation 2.3.

$$\mathrm{TiCl_4(g) + 2\,Mg\,(l) \longrightarrow Ti\,(s) + 2\,MgCl_2(l)} \tag{2.3}$$

As the reduction proceeds, $MgCl_2$ is periodically tapped off, and when the pressure in the stainless steel container rises, the reaction stops [3]. The container now contains unreacted Mg, and a titanium metal porous sponge with some $MgCl_2$ trapped in the pores. To purify the metal sponge, leaching or vacuum distillation is applied to remove the Mg and $MgCl_2$. Then the pure titanium is melted and solidified to produce an ingot. The duration of the reduction is dependent on the size of the container, though normally it requires three to four days [4]. The reduction reaction is strongly exothermic, and controlling the heat balance is difficult [19]. The container has to be cooled in order to control the temperature, which is limiting the batch size. Both Mg and $MgCl_2$ have to be in the liquid state, putting a limit on the temperature range of the reaction [20]. The lower limit is the melting point of $MgCl_2$ (714°C [21]), and the upper limit is the boiling point of Mg (1110°C [21]). Therefore, the industrial production temperature is kept between 850°C and 900°C, giving some headroom from the absolute limiting temperatures and preventing contamination of iron from the container walls.

Regeneration step

$MgCl_2$ generated in the reduction step is recycled in a fused salt electrolysis process which produces Mg and Cl_2 gas according to Equation 2.4 [22]. The Cl_2 gas is reused in the chlorination step and the Mg in the reduction of $TiCl_4$. The electrolysis is carried out at 750°C in a NaCl−$CaCl_2$ based melt which has a higher density than Mg. Therefore, Mg will float on top and can be tapped out at regular intervals.

$$\mathrm{MgCl_2(dissolved)} \longrightarrow \mathrm{Mg\,(l)} + \mathrm{Cl_2(g)} \tag{2.4}$$

This step itself is energy demanding, and the most modern cells have an energy consumption of ∼15 kWh/kg Mg and contributes to the overall complexity of the Kroll process.

2.2 New emerging technology

In the years after the invention of the Kroll process, many researchers made an attempt to develop a new electrochemical route for titanium production [23]. The FFC Cambridge process and the Armstrong process are some of the most promising approaches and will be described in Section 2.2.1 and Section 2.2.2, respectively, along with the work by Ginatta *et al.* [24] in Section 2.2.3.

The main obstacle for an electrochemical route is to fulfil the purity requirements. This challenge arises due to the lack of an inert oxygen evolving anode, and problems with the existence of various oxidation states of dissolved titanium species [23]. Titanium forms stable compounds and can exist as Ti(II), Ti(III), and Ti(IV). Ti(IV) has low solubility in molten salts, and most research has used Ti(II) and Ti(III) as the titanium source. All these oxidation states give rise to the following electrochemical reduction steps:

$$\mathrm{Ti(IV)} + \mathrm{e^-} \longrightarrow \mathrm{Ti(III)} \tag{2.5}$$

$$\mathrm{Ti(III)} + \mathrm{e^-} \longrightarrow \mathrm{Ti(II)} \tag{2.6}$$

$$\mathrm{Ti(II)} + 2\,\mathrm{e^-} \longrightarrow \mathrm{Ti} \tag{2.7}$$

Titanium can be produced in molten chlorides from Ti(II), which is not stable in molten salts containing fluoride, and disproportionation reactions such as Equation 2.8 can occur.

$$3\,\mathrm{Ti(II)} \longrightarrow 2\,\mathrm{Ti(III)} + \mathrm{Ti} \tag{2.8}$$

The main problem with this is the possible cycling between the different oxidation states that can ruin the current efficiency and also interfere with the deposit at the cathode.

2.2.1 The FFC Cambridge process

Fray, Farthing and Chen published an innovative article in 2000, describing a process to produce titanium electrochemically from TiO_2, which today is known as the FFC Cambridge process [11]. In the original article, a graphite anode was used, and TiO_2 was polarised cathodically in a molten $CaCl_2$ electrolyte. The oxide ions diffuse into the melt as O^{2-} and combine with the carbon anode and form CO and CO_2 gas which escapes from the cell. If an inert anode could replace the graphite anode, oxygen gas could be produced instead of the harmful environmental gasses. The total cathodic reaction is given in Equation 2.9, the anode reaction in Equation 2.10, and Figure 2.2 shows a schematic drawing of two proposed cell designs.

$$\mathrm{TiO_2(s)} + 4\,\mathrm{e^-} \longrightarrow \mathrm{Ti\,(s)} + 2\,\mathrm{O^{2-}(dissolved)} \tag{2.9}$$

$$\mathrm{C\,(s)} + 2\,\mathrm{O^{2-}(dissolved)} \longrightarrow 4\,\mathrm{e^-} + \mathrm{CO_2(g)} \tag{2.10}$$

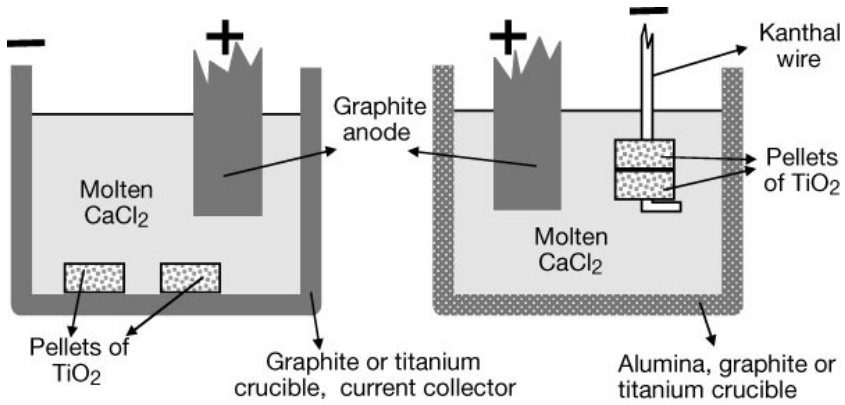

Figure 2.2: Two proposed cell designs for the FFC Cambridge process sourced from [11].

This process does not require a melt to dissolve titanium, the problems associated with multivalent titanium are eliminated. However, findings from subsequent research studies revealed several issues with this process. For instance, Chen and Fray published another article in 2004, where they discussed the possibility of back reactions, which gives current losses and poor quality of the end product due to high oxygen content [25]. Additionally, they addressed problems related to the balance of O^{2-} distribution between the anode and cathode due to slow kinetics, as the oxygen is needed at the anode and low oxygen activity is desired at the cathode.

After the invention of the FFC Cambridge process, work on trying to scale up the process was carried out [26]. Among them, a company from Cambridge University, British Titanium plc, was granted a licence for producing titanium and alloys containing more than 40 mass% titanium. Experiments were carried out but showed problems with low current efficiency, inconsistencies in product quality, and dendrite formations. However, a collaboration between Cambridge University, British Titanium, Norsk Titanium and Norsk Hydro showed promising results. By controlling the applied potential throughout the experiments, they managed to reduce a batch of TiO_2 in less than one day. Unfortunately, this collaboration ended in 2005 when the British Titanium licence terminated. British Titanium continued working, but after this, they focused more on inert anode technology. The main issues with the FFC Cambridge process on a larger scale basis are the use of carbon based anodes. As the carbon is consumed, particles can erode from the anode and build up as sludge in the electrolyte, which can cause short-circuit of the cell [26]. Secondly, the lack of a suitable anode for oxygen evolution causes a problem with the evolving CO_2. Because CO_2 may dissolve as CO_3^{2-} ions in the electrolyte, diffuse to the cathode and discharge according to Equation 2.11. The deposited

carbon may contaminate the product and cause a drop in the current efficiency.

$$CO_3^{2-}(\text{dissolved}) + 4\,e^- \longrightarrow C\,(s) + 3\,O^{2-}(\text{dissolved}) \tag{2.11}$$

The OS process and The PR process

Two similar methods to the FFC Cambridge process are the OS process developed by Suzuki *et al.* [27], and the PR process developed by Okabe *et al.* [28]. What distinguishes these methods from the FFC Cambridge process are different reactor designs and reaction mechanisms.

The OS process is based on a calciothermic reduction of titanium dioxide powder to gain metallic titanium [27]. Ca is dissolved in a fused $CaCl_2$ melt, containing the by-product CaO. With a carbon anode, CO_2 will be evolved, and Equation 2.10 shows the proposed anode reaction, and the cathodic reaction is believed to be following Equation 2.12.

$$Ca^{2+}(\text{dissolved}) + e^- \longrightarrow Ca^{+}(\text{dissolved}) \tag{2.12}$$

The cathode product, which may exist as ${Ca_2}^{2+}$, reacts with TiO_2 according to Equation 2.13.

$$\begin{gathered} TiO_2(s) + 2\,Ca^{+}(\text{dissolved}) + 2\,e^- \longrightarrow \\ Ti\,(s) + 2\,Ca^{2+}(\text{dissolved}) + 2\,O^{2-}(\text{dissolved}) \end{gathered} \tag{2.13}$$

The Ca^{2+} ions migrate in the molten $CaCl_2$, and when the melt is saturated, liquid calcium can be deposited at the cathode according to Equations 2.14 and 2.15.

$$Ca^{2+}(\text{dissolved}) + 2\,e^- \longrightarrow Ca\,(l) \tag{2.14}$$

$$Ca^{+}(\text{dissolved}) + e^- \longrightarrow Ca\,(l) \tag{2.15}$$

TiO_2 will react with the calcium droplets and is reduced according to the following reaction in Equation 2.16.

$$\mathrm{TiO_2(s)} + 2\,\mathrm{Ca\,(l)} \longrightarrow \mathrm{Ti\,(s)} + 2\,\mathrm{Ca^{2+}(dissolved)} + 2\,\mathrm{O^{2-}(dissolved)} \tag{2.16}$$

The main problems with this process are the poor current efficiency due to deposition of calcium metal, and similar to the FFC process, the lack of an O_2 evolving anode which causes problems with carbonates.

The preform reduction process (PRP) is also a calciothermic reduction process but uses calcium vapour to reduce TiO_2 preforms [28]. The reduction takes place in a sealed stainless steel container, containing the TiO_2 preforms and solid calcium. The temperature ranges between 800°C-1000°C, and by acid leaching the reduced preforms, titanium powder is recovered. The product quality will be dependent on the preforms composition and size. However, this process is suitable to produce a homogeneous fine powder if these parameters are controlled. Figure 2.3 shows a schematic illustration of the reactor vessel, and the reaction is claimed to follow Equation 2.17.

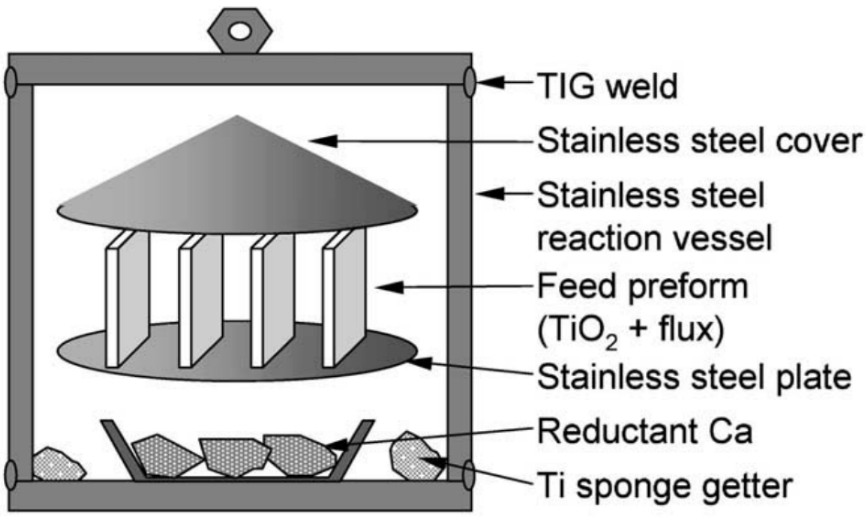

Figure 2.3: A schematic illustration of the experimental reaction vessel for producing titanium powder by the PR process sourced from [28].

$$\mathrm{TiO_2(s)} + 2\,\mathrm{Ca\,(g)} \longrightarrow 2\,\mathrm{CaO\,(s)} + \mathrm{Ti\,(s)} \tag{2.17}$$

2.2.2 The Armstrong process

Another promising process, with a potential to reduce the titanium price, is the Armstrong process developed by International Titanium Powder [3]. Similar to the Hunter process, sodium is used as the reduction agent. However, this process is continuous rather than a batch process, which makes it more efficient. Additionally, the end product is titanium powder and not a titanium sponge as in the Kroll process. $TiCl_4$ vapour is reduced by a stream of excess molten sodium. The excess sodium is cooling the reaction product and acts as a carrier to the separation stage where salt and sodium are removed and can be reused. Titanium powder is continuously produced, and with modifications, vanadium/aluminium titanium alloys can be made by this method. The main advantage of this process is the continuity, which will contribute to reducing the price. However, some of the remaining challenges are the high cost of producing Na and $TiCl_4$, and the small particle size giving the produced metal high reactivity.

2.2.3 GTT

Marco Ginatta worked on industrialising an electrochemical process for titanium production in the 1980s [24]. The process is a two-step reduction of $TiCl_4$ to pure Ti, in a molten NaCl based melt, according to Equation 2.18 and 2.19.

$$\mathrm{TiCl_4(g)} \longrightarrow \mathrm{TiCl_2(g)} + \mathrm{Cl_2(g)} \tag{2.18}$$

$$\mathrm{TiCl_2(g)} \longrightarrow \mathrm{Ti\,(s)} + \mathrm{Cl_2(s)} \tag{2.19}$$

He built a big pilot plant in Torino, Italy, and his work resulted in two patents [29,30]. As more titanium became available after the cold war, the titanium prices dropped [19]. Combined with the high production costs, this led to the end of the pilot plant as it became too expensive to continue with this research.

2.2.4 Producing titanium by use of liquid Bi

Kado *et al.* [31] are currently working on a new smelting process for titanium production utilising a liquid Bi. In 2013, they published a paper proposing a continuous smelting process, where TiO_2 is reduced into liquid Bi cathode in molten

$CaCl_2$, forming Bi−Ti liquid alloys followed by electrorefining or vacuum distillation to gain pure titanium metal [31]. The operating temperatures range between 900°C-1000°C, and the alloy is liquid, meaning the reduction step and the refining step can be carried out continuously, in contrast to the Kroll process. Additionally, will this lead to a higher production rate of titanium. For the refining step, vacuum distillation will probably be the best choice for an industrial process due to low energy consumption compared to electrorefining. However, the method showed some problems with co-deposition of Ca into the liquid Bi, due to low activity of Ca in Bi, which inhibited the formation of Bi−Ti alloy. However, results showed a relatively small Ca contamination when $TiCl_2$ was used instead of TiO_2. By consideration based on the potential-pO^{2-} diagram for the Ti−Ca−O−Cl system, they found that it is important to keep a low O^{2-} concentration in the electrolyte to obtain Bi−Ti alloy with low Ca contamination. This is difficult due to fomation of O^{2-} ions at the Bi cathode during reduction of TiO_2.

2.2.4.1 Modification of the Kroll process

In 2014, Kado *et al.* [1] published a paper demonstrating another alternative process for titanium production [1]. The method is based on the current Kroll process, and Mg reduces $TiCl_4$ into a liquid Bi cathode, according to Equation 2.20. Similar to the method described above, Bi−Ti alloy is formed, followed by a refining step where the reduction step and refining step can be carried out continuously, leading to an increased productivity of Ti. In this process, the formed alloy is subsequently refined by vacuum distillation, and Figure 2.4 shows a schematic illustration of the process. They also estimated the cooling effect of Bi in the reduction step, as the magnesiothermic reduction of $TiCl_4$ is highly exothermic. They did so by considering the heat balance for the reduction step, for more details see reference [1], and their study showed that the new alternative process has the potential to improve the feed rate of $TiCl_4$ when the concentration of Ti in the alloy is between 6-7 at.%. In addition to the continuity, this can contribute to an even higher productivity of titanium. Overall the process is very similar to the Kroll process besides the use of liquid Bi. Parts of the equipment used can be utilised in this alternative process, such as the equipment for recycling the generated $MgCl_2$, and for the carbochlorination of TiO_2. Additionally, Bi can be reused after the vacuum distillation.

$$\mathrm{TiCl_4(g)} + 2\,\mathrm{Mg(in\,Bi)} \longrightarrow \mathrm{Ti(in\,Bi)} + 2\,\mathrm{MgCl_2(l)} \tag{2.20}$$

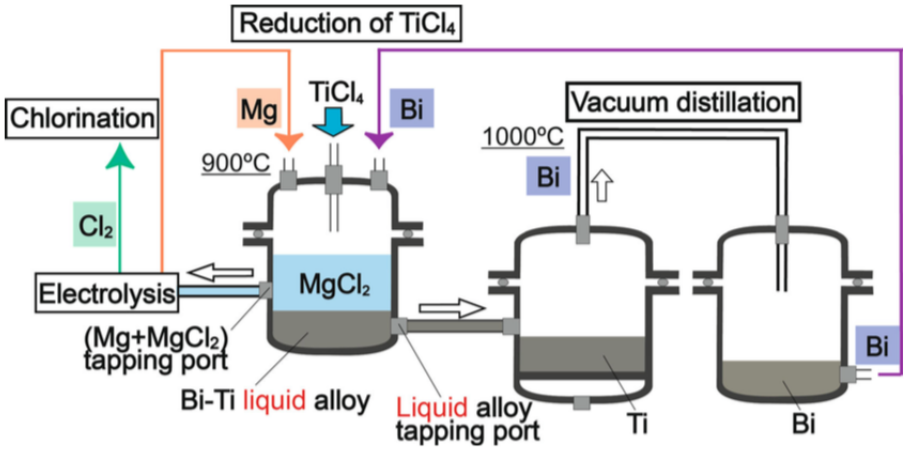

Figure 2.4: A schematic illustration of a proposed new process, with vacuum distillation as the refining step, developed at Kyoto University sourced from [1].

They also experimentally investigated the magnesiothermic reduction of $TiCl_4$ and refining of Ti by vacuum distillation. The experimental work on magnesiothermic reduction was carried out in MgO crucible with mixtures at several compositions of Mg and Bi [1]. The mixtures were heated up to 750°C or 900°C under Ar atmosphere, followed by an addition of $TiCl_4$. Then the temperature was maintained for one hour at 750°C, 900°C or 1000°C. By EDX analysis and assuming the reaction proceeded entirely, they calculated the theoretical amount of Ti in the alloys from the nominal compositions. The content of Ti in the alloys was determined to range from 7.9 at.% to 33.4 at.%. To be able to separate the alloy from $MgCl_2$, the concentration of Ti in the liquid alloy should be sufficiently lower than the solubility of Ti in Bi. This avoids the formation of unwanted compounds that can adhere to the crucible wall (see reference [1]).

To investigate vacuum distillation, they first prepared homogeneous Bi−Ti alloy by mixing Bi and Ti with ratio of 65:53 at.% [1]. The mixture was then annealed to 1000°C in a closed cell and subsequently quenched in water. Vacuum distillation at 1000°C was performed on the prepared alloy for 24 hours. By examining the obtained Ti by EDX, they found a purity as high as 99.6 at%, which indicated that vacuum distillation could be a viable refining technique. However, further investigation is still required in order to implement an efficient continuous process. Since the Ti concentration is low in the alloy obtained after the reduction step, they suggested that segregation may increase the Ti concentration before the vac-

uum distillation.

Kishimoto *et al.* [32] published a paper in 2016 that investigated the electrorefining of Ti from Bi−Ti alloy at 700°C for production of titanium by use of a liquid Bi cathode. They used a Bi−Ti anode and a Ni cathode in equimolar NaCl−KCl melt and added $TiCl_2$ [32]. They obtained a highly pure Ti powder with the Bi contamination was below 180 ppm, and with a current efficiency above 90%. The production route of this process is very similar to the alternative process suggested in 2014, but with electrorefining instead of vacuum distillation as the refining step. Figure 2.5 shows a schematic illustration of this proposed process.

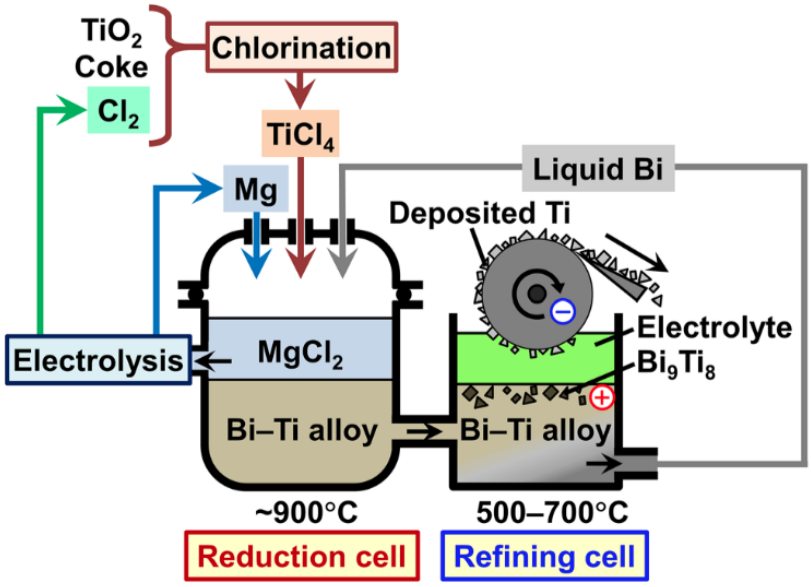

Figure 2.5: A schematic illustration of a proposed new process, with electrorefining as the refining step, developed at Kyoto University sourced from [32].

In this process, the liquid alloy is transported to the refining cell where Ti is obtained. The production rate is enhanced by continuously unpeeling the deposited Ti with a rotating cylinder-shaped cathode and transferring the Ti from the reduction cell to the refining cell. They claimed that the electrorefining of Ti, using Bi−Ti alloy anode, will proceed according to Equations 2.21 and 2.22.

$$\mathrm{Ti(in\,Bi{-}Ti)} \longrightarrow \mathrm{Ti^{3+}} + 3\,\mathrm{e^-} \tag{2.21}$$

$$\mathrm{Ti}^{3+} + 3\,\mathrm{e}^- \longrightarrow \mathrm{Ti(pure)} \tag{2.22}$$

The bismuth in the alloy anode can be oxidised according to Equation 2.23, which should be avoided due to contamination of the cathode product.

$$\mathrm{Bi(in\,Bi{-}Ti)} \longrightarrow \mathrm{Bi}^{3+} + 3\,\mathrm{e}^- \tag{2.23}$$

Due to the several oxidation states of Ti, and the lack of research on the anodic behaviour of Bi−Ti alloy, the conditions for an effective electrorefining is still unclear and more research should be carried out.

Chapter 3

Theory

Several authors have been investigating the use of a liquid cathode to produce Ti-M alloys, where M is the metal, and Gleave *et al.* [33] studied a process involving Ti−Zn alloy. Various other metals have also been suggested to be suitable for alloying with Ti, e.g., Cu, Cd, Ni, Sn, Zn, Pb, and Bi [32].

For a magnesiothermic reduction of Ti into a liquid alloy, it is important to form a liquid alloy with a Ti concentration far from the solubility in order to get efficient separation from $MgCl_2$ [1]. From the phase diagram shown in Figure 3.1 [34], we can see that Ti has a solubility of around 30 at.% in Bi at 900°C. In comparison to the Ti−Zn system where the solubility is around 11.5 at.% at 900°C, Bi is a better candidate according to the phase diagram shown in Figure 3.2 [35]. The vapour pressure of Zn and Bi is 9.5×10^{-1} atm and 1.9×10^{-3} atm, respectively [1]. Kado *et al.* [1] believed that a lower vapour pressure is beneficial for the reduction step of the proposed process, suggesting that Bi is a suitable alloy element. An additional feature of Bi is the low melting point (271°C [21]) which makes it easy to keep the solvent metal in the liquid state.

Thermodynamics can be used to predict whether such a system is in equilibrium and to analyse the phase stability and phase transformation. In this thesis, we look at Bi−Ti alloys which are systems consisting of a mixture of two different chemical components, and hence binary solutions. In a binary solution, only two components are present, which is a particular case of the more general multicomponent system. A binary system may be in liquid state, or a solid solution. In the case of a solid solution, the excess component is referred to as the solvent, and the minor component is called the solute. In this chapter some fundamental thermodynamics will be presented, followed by the thermodynamics of solutions with a focus on binary systems.

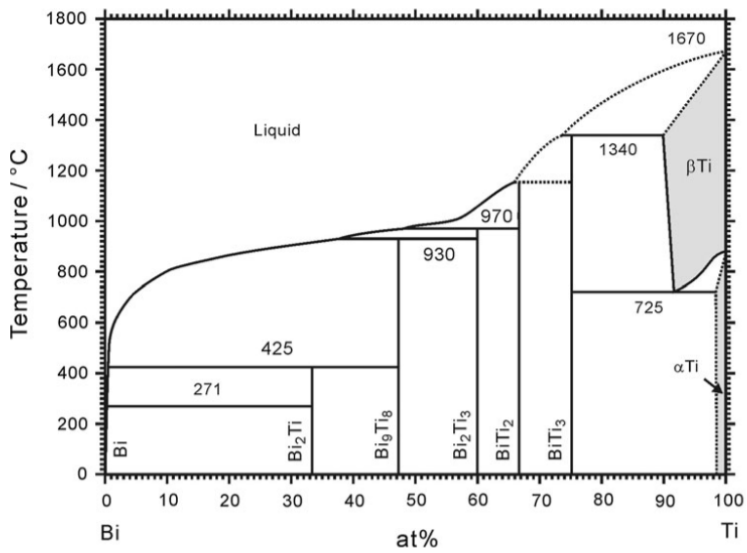

Figure 3.1: Phase diagram of the Bi−Ti binary system sourced from [34].

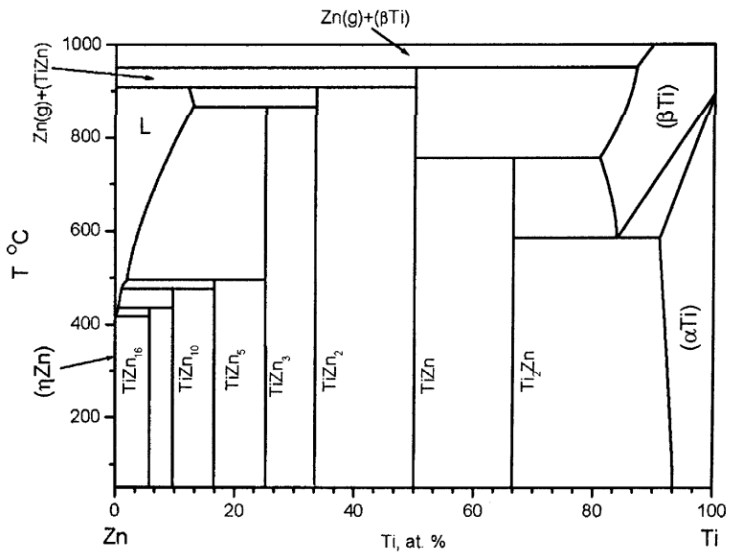

Figure 3.2: Phase diagram of the Ti−Zn binary system sourced from [35].

3.1 Gibbs energy

Gibbs energy is an important property in thermodynamics, and it is a measure of the theoretical maximum work that is possible to get out of a closed system at constant pressure and temperature [36]. This property also serves as a practical criterion for spontaneity for processes at constant temperature and pressure. Gibbs energy of a system is related to the enthalpy and entropy of the system as given in Equation 3.1. Enthalpy is a function of temperature and is a measure of the energy in a system, and entropy can be looked upon as a measure of the disorder in a system.

$$G = H - TS \tag{3.1}$$

G is Gibbs energy, H is enthalpy, S is entropy and T is the temperature, and the change in Gibbs energy for the system can consequently be described by Equation 3.2 at constant temperature.

$$dG = dH - TdS \tag{3.2}$$

For a spontaneous change, dG will have a negative value at constant temperature and pressure, in the direction of decreasing Gibbs energy for a chemical reaction. The total differential for Gibbs energy is given in Equation 3.3 and describes how the Gibbs energy changes with pressure, p, and temperature, T, at constant composition in a closed system in the absence of non-expansion work. Meaning the volume, V, is constant.

$$dG = Vdp - SdT \tag{3.3}$$

From Equation 3.3 we can see how Gibbs energy varies with temperature and pressure. Equation 3.4 and Equation 3.5 show this at isobaric and isothermal conditions, respectively.

$$\left(\frac{\partial G}{\partial T}\right)_P = -S \tag{3.4}$$

$$\left(\frac{\partial G}{\partial p}\right)_T = V \tag{3.5}$$

3.1.0.1 The variation of the Gibbs energy with pressure

The Gibbs energy at one pressure relative to its value at another pressure can be found by integrating Equation 3.3, at a constant temperature which leads to Equation 3.6 [36].

$$G(p_f) = G(p_i) + \int_{p_i}^{p_f} V dp \tag{3.6}$$

$G(p_f)$ is the Gibbs energy at the final pressure p_f, and $G(p_i)$ is the Gibbs energy at the initial pressure p_i, and V is the volume. This expression can be applied to any phase of matter, and for an ideal gas, it is convenient to express the volume in terms of the ideal gas law which is expressed as:

$$pV = nRT \tag{3.7}$$

where p is pressure, V is volume, n is the number of mole, T is the temperature, and $R = 8.314\,[\mathrm{J/(K \cdot mol)}]$ the gas constant. This law is valid for ideal gases, but can be applied at low pressures and is based on a series of empirical laws. In these cases, the volume in Equation 3.6 can be replaced by a rearrangement of the gas law and becomes:

$$G(p_f) = G(p_i) + nRT \int_{p_i}^{p_f} \frac{1}{p} dp = G(p_i) + nRTln\frac{p_f}{p_i} \tag{3.8}$$

By putting the initial pressure, p_i, equal to the standard pressure, $p^0 = 1\,\mathrm{bar}$, we get the expression in Equation 3.9, where the Gibbs energy for gas is expressed with the standard state as a reference state and G^0 is the standard Gibbs energy.

$$G(p_f) = G^0 + nRTln\frac{p_f}{p^0} \tag{3.9}$$

3.2 The behaviour of solutions

At sufficiently high temperature and sufficiently low pressure, a mixture of gases can be considered ideal since the interactions among the atoms and molecules are small and therefore negligible [37]. Consequently, all mixtures of gases will have the same thermodynamic mixing properties at high enough temperature and low enough pressure. In condensed solutions, there are strong interactions between

atoms, molecules, or ions. The magnitudes and nature of these interactions will influence the thermodynamic behaviour of the solution, and the interactions are determined by factors such as atomic size, electronegativity and electron-to-atom ratio. These factors will determine how components will behave in a solution, such as if a component is soluble in a solution or if the components can react chemically to form separate chemical compounds. In thermodynamics of solution the relationship between vapour pressure, temperature and composition of the components of a solution is of interest, and in this section, an examination of solution thermodynamics will be given.

3.2.0.1 Raoult's law

Raoult's law is valid for all ideal solutions but will never be exact for real solutions [36]. This law can be used when the deviation from ideality is small, and for many cases, it will be valid. It is most valid for mixtures where the different components have the same structures on a molecular level, or for excess components. The law states that the partial vapour pressure of component i, in an ideal liquid mixture is equal to the product of the components mole fraction in the liquid and the vapour pressure of the pure component at a certain temperature. In mathematical terms, this can be expressed as in Equation 3.10. The vapour pressure is the pressure of a vapour of component i, in its condensed phase.

$$p_i = x_i \cdot p_i^* \tag{3.10}$$

In Equation 3.10, p_i is the partial vapour pressure of component i above the ideal mixture, x_i is the mole fraction of component i in liquid phase, and p_i^* is the vapour pressure of pure component i at a certain temperature. If the components of a solution obey Raoult's law, they are said to exhibit Raoultian behaviour, and the behaviour of component i approaches Raoult's law as $x_i \rightarrow 1$ in solution.

3.2.0.2 Henry's law

For a binary solution, Henry's law is obeyed by the solute in the composition range where the solvent obeys Raoult's law [37]. Henry's law states that the partial pressure of component i over a solution is proportional to the amount of gas dissolved, this can be expressed as in Equation 3.11.

$$p_i = k^{'} \cdot x_i \tag{3.11}$$

In Equation 3.11, p_i is the partial pressure in the gas phase of component i, x_i is the mole fraction of component i, and $k^{'}$ is called Henry's law constant and is empirical. Components of a solution that obey Henry's law are said to exhibit Henrian behaviour, and the behaviour of component i approaches Henry's law as $x_i \rightarrow 0$ in solution.

3.3 Partial molar properties

Extensive properties, such as enthalpy, volume, entropy and Gibbs energy, are not the sum of those properties of the unmixed components upon mixing [37]. Therefore, partial molar quantities are used to describe the individual behaviour of each component in the system in a given phase.

If we have the extensive property Q of component i, in a mixture of components i, j, $k\ldots$ the partial molar quantities will be defined as:

$$\bar{Q}_i = \left(\frac{\partial Q}{\partial n_i}\right)_{T,P,n_j,n_k\ldots} \tag{3.12}$$

where $\bar{Q}_i$ is the rate of change of value Q with the number of moles of component i, n_i, at constant temperature and pressure, and with all other present substances being constant. An important molar quantity is the chemical potential which is defined as:

$$\mu_i = \left(\frac{\partial G}{\partial n_i}\right)_{T,P,n_j,n_k\ldots} \tag{3.13}$$

where G is Gibbs free energy, and μ_i is the chemical potential of component i. The chemical potential can be looked upon as the driving force for chemical reactions, and its value depends on the composition of the solution.

3.4 The Gibbs-Duhem equation

In a binary solution the extensive thermodynamic properties of one component can be found through experimental measurements. Given the relationship between the two components, the properties corresponding to the second component can be

obtained [37]. This relationship is known as the Gibbs-Duhem equation and will be presented in this section. An extensive thermodynamic property of a solution is a function of temperature, pressure and number of moles of the components. For simplicity, the following explanations will be given for a two component system, but generally this can also be applied to multicomponent systems. If Q_m is the extensive molar property, it can be expressed as:

$$Q_m = Q_m(T, P, n_i, n_j) \tag{3.14}$$

where T is temperature, P is pressure, n_i and n_j are the number of moles of component i and j respectively. The change in Q at constant T and P, can be described as:

$$dQ_m = \left(\frac{\partial Q}{\partial n_i}\right)_{T,P,n_j} \cdot dn_i + \left(\frac{\partial Q}{\partial n_j}\right)_{T,P,n_i} \cdot dn_j \tag{3.15}$$

and by combining this expression with Equation 3.12, Equation 3.15 can be expressed as:

$$dQ_m = \bar{Q}_i dn_i + \bar{Q}_j dn_j \tag{3.16}$$

since $\bar{Q}_i$ is the value of Q per mole of i in the solution, the value of Q_m itself in the solution can be expressed as in Equation 3.17.

$$Q_m = \bar{Q}_i n_i + \bar{Q}_j n_j \tag{3.17}$$

Differentiation of Equation 3.17 then gives:

$$dQ_m = d\bar{Q}_i n_i + d\bar{Q}_j n_j + \bar{Q}_i dn_i + \bar{Q}_j dn_j \tag{3.18}$$

and by comparing Equation 3.16 and Equation 3.18, it follows that:

$$d\bar{Q}_i n_i + d\bar{Q}_j n_j = 0 \tag{3.19}$$

at constant T and P. In general, this can be expressed by Equation 3.20 or in terms of the mole fractions, x_i, of the components as in Equation 3.21. These two expressions are equivalent expressions of the Gibbs-Duhem equation at constant T and P.

$$\sum_i n_i d\bar{Q}_i = 0 \tag{3.20}$$

$$\sum_i x_i d\bar{Q}_i = 0 \tag{3.21}$$

Relation between the molar Gibbs energy of the solution, and the partial molar Gibbs energy of the components

The molar Gibbs energy, G_m, for a binary solution with component A and B at constant temperature and pressure can be described by Equation 3.17 giving Equation 3.22 [37].

$$G_m = \bar{G_A} n_A + \bar{G_B} n_B \tag{3.22}$$

In Equation 3.22, $\bar{G_A}$ and $\bar{G_B}$ are the partial molar Gibbs energy of component A and B respectively, and n_A and n_B are the number of moles of component A and B respectively. By using the expression in Equation 3.13, substituting the partial molar Gibbs energy of each component, with their chemical potential, μ_i, Equation 3.22 can be expressed as:

$$G_m = \mu_A n_A + \mu_B n_B \tag{3.23}$$

or in terms of the mole fractions, x_i, by dividing Equation 3.23 by the total number of moles, $n = n_A + n_B$, giving Equation 3.24.

$$G_m = \mu_A x_A + \mu_B x_B \tag{3.24}$$

By differentiation of Equation 3.24 and application of the Gibbs-Duhem equation, we get the relation between the chemical potential and change in Gibbs energy of a binary system as shown in Equation 3.25.

$$dG_m = \mu_A dx_A + \mu_B dx_B \tag{3.25}$$

As $x_A + x_B = 1$ it follows that $dx_B = -dx_A$ and Equation 3.25 can be rearranged to Equation 3.26.

$$\frac{dG_m}{dx_A} = \mu_A - \mu_B \tag{3.26}$$

By multiplying Equation 3.26 with x_B and then adding Equation 3.26 to Equation 3.24, the expression in Equations 3.27 and 3.28 are obtained. These two expressions show the relation between the molar Gibbs energy of the solution and the partial molar Gibbs energy of the components in a binary solution.

$$\mu_A = G_m + x_B \frac{dG_m}{dx_A} \tag{3.27}$$

$$\mu_B = G_m + x_A \frac{dG_m}{dx_B} \tag{3.28}$$

3.5 Mixing of solutions

Solids, liquids or gases can be combined to form a mixture, and as a result, the thermodynamic quantities of the system will experience a change [36]. This section will present how Gibbs energy, enthalpy and entropy will change upon mixing of ideal gases, and later for ideal solutions.

3.5.0.1 Mixing of ideal gases

It is assumed that in an ideal gas there are no interactions between the molecules [36]. Starting by expressing Equation 3.9 by molar Gibbs energy, which is achieved by dividing it by the total number of moles, n, giving Equation 3.29.

$$G_m = G_m^0 + RTln\frac{p}{p^0} \tag{3.29}$$

In Equation 3.29, G_m is the molar Gibbs energy, and G_m^0 is the standard molar Gibbs energy of the gas at $p^0 = 1$ bar pressure, and p is the pressure of the system. For a system with more than one component, the partial molar Gibbs energy is equal to chemical potential for component i. Equation 3.29 can be expressed in terms of the chemical potential of component i, given in Equation 3.30.

$$\bar{G}_i = \mu_i = \mu_i^0 + RTln\frac{p_i}{p^0} \tag{3.30}$$

In Equation 3.30, μ_i is the chemical potential for component i, μ_i^0 is the standard chemical potential for component i at $p^0 = 1\,\text{bar}$ pressure, and p_i is the partial pressure of component i. Now looking at two gases, say gas A and B, with the same pressure, p, at the same temperature, the total Gibbs energy of the system before mixing is described by combining Equation 3.24 and Equation 3.30 giving Equation 3.31.

$$G_{m,initial} = x_A(\mu_A^0 + RTln\frac{p}{p^0}) + x_B(\mu_B^0 + RTln\frac{p}{p^0}) \tag{3.31}$$

After gas A and B are mixed together, they will each exert a partial pressure on the system, and the final Gibbs energy of the system can be described by Equation 3.32.

$$G_{m,final} = x_A(\mu_A^0 + RTln\frac{p_A}{p^0}) + x_B(\mu_B^0 + RTln\frac{p_B}{p^0}) \tag{3.32}$$

From these two expressions the molar Gibbs energy of mixing, $\Delta_{mix}G_m$, can be found by subtracting Equation 3.31 from Equation 3.32 giving Equation 3.33.

$$\Delta_{mix}G_m = G_{m,final} - G_{m,initial} = x_A RTln\frac{p_A}{p} + x_B RTln\frac{p_B}{p} \tag{3.33}$$

Using the relations between partial pressure, p_i, mole fraction, x_i, and the total pressure of the system, p, $p_i = x_i p$, $\Delta_{mix}G_m$ can be expressed by Equation 3.34.

$$\Delta_{mix}G_m = RT(x_A lnx_A + x_B lnx_B) \tag{3.34}$$

Since x_A and x_B are the mole fractions and therefore less than 1, we conclude that the Gibbs energy of mixing must be negative, and gases mix spontaneously at constant pressure and temperature. From Equation 3.4 and Equation 3.34 it follows immediately that the molar entropy of mixing, $\Delta_{mix}S_m$, for gas must be:

$$\Delta_{mix}S_m = \left(\frac{\partial \Delta_{mix}G_m}{\partial T}\right)_{P,n_A,n_B} = -R(x_A lnx_A + x_B lnx_B) \tag{3.35}$$

Here the mole fractions lead to a negative value, and due to the negative sign, $\Delta_{mix}S_m$ must be positive, which implies that a mixing leads to more disorder in the system. The relation given in Equation 3.1 can be applied to the thermodynamics of mixing, and combined with Equation 3.34 and Equation 3.35 the molar enthalpy of mixing, $\Delta_{mix}H_m$, can be derived as demonstrated in Equation 3.36.

$$\Delta_{mix}H_m = RT(x_A lnx_A + x_B lnx_B) + T[-R(x_A lnx_A + x_B lnx_B)] = 0 \tag{3.36}$$

Considering a system with ideal gases, this demonstrates that no heat is produced nor absorbed, and it is reasonable to assume that in an ideal gas the molecules are so spread that they do not interact with each other when mixing.

3.5.0.2 Mixing of ideal solutions

In this part, the change in the thermodynamic properties, Gibbs energy, entropy and enthalpy upon mixing for ideal binary solutions will be presented [36]. To discuss the equilibrium properties of liquid mixtures, the fact that $\mu_i(l)$ is equal to $\mu_i(g)$ at equilibrium is used. This holds true since the chemical potential of component i in the vapour is dependent on its partial vapour pressure. Now looking further into the case where two liquids are mixed, and for an ideal solution, the Gibbs energy of mixing can be calculated in the same way as for ideal gases. In the following, the quantities relating to pure substances will be denoted by a script $*$, for example, the chemical potential of pure A is written μ_A^*.

Since, in this case, liquids are of interest, the pure liquid state is the reference state chosen for each component. Equation 3.30 can be written as in Equation 3.37, for the individual components in the system of an ideal solution.

$$\mu_i = \mu_i^* + RTln\frac{p_i}{p_i^*} \tag{3.37}$$

In Equation 3.37, μ_i is the chemical potential of component i in the mixture, μ_i^* is the chemical potential of component i in its pure state, p_i is the partial vapour pressure of component i in the vapour over the mixture, and p_i^* is the partial vapour pressure of component i over pure i.

The total molar Gibbs energy of the system with two liquids A and B before mixing can now be expressed by Equation 3.38 and after mixing by Equation 3.39.

$$G_{m,initial} = x_A(\mu_A^* + RTln\frac{p}{p_A^*}) + x_B(\mu_B^* + RTln\frac{p}{p_B^*}) \tag{3.38}$$

$$G_{m,final} = x_A(\mu_A^* + RTln\frac{p_A}{p_A^*}) + x_B(\mu_B^* + RTln\frac{p_B}{p_B^*}) \tag{3.39}$$

The same derivation in the case of mixing two ideal gases is applied in the case of mixing two ideal liquids and $\Delta_{mix}G_m$, $\Delta_{mix}S_m$ and $\Delta_{mix}H_m$ for liquids are the same as given in Equation 3.34, 3.35 and 3.36 respectively.

It should be noted that an ideal solution differs from an ideal gas since there are interactions in an ideal solution. To illustrate, consider a system with two types of molecules in a solution, A and B. There are interactions between A-A, A-B and B-B, and for an ideal solution, the average interactions between A-B in the mixture is assumed to be the same as for the A-A and B-B interactions in pure liquids. However, in the case for real solutions, these interactions may all be different, and the change in enthalpy of mixing may no longer be zero.

3.5.0.3 Activity and activity coefficient

The chemical potential of a substance i, in an ideal mixture, can be described using Raoult's law, and the chemical potential given in Equation 3.37 can then be expressed by Equation 3.40 for component i in a liquid solution [36].

$$\mu_i = \mu_i^* + RTlnx_i \tag{3.40}$$

The term activity, a_i, and the activity coefficient, γ_i, are introduced to express the chemical potential of component i in a non-ideal solution. For a non-ideal solution, Equation 3.40 is expressed as:

$$\mu_i = \mu_i^* + RTlna_i \tag{3.41}$$

where a_i is the activity of component i, and it is defined by Equation 3.40 for an ideal solution. As $x_i = \frac{p_i}{p_i^*}$, the activity of component i is also given by Equation 3.42, and the relation between the activity and the activity coefficient is shown in Equation 3.43.

$$a_i = x_i = \frac{p_i}{p_i^*} \tag{3.42}$$

$$a_i = \gamma_i x_i \tag{3.43}$$

The activity coefficient is a measure of how much an actual system deviates from an ideal solution. This deviation can be either positive or negative relative to an

ideal solution, and when $\gamma_i = 1$ for component i we have an ideal solution. The activity of component i can be found experimentally by measuring the vapour pressure, p_i of component i, in a binary solution, by using the relation given in Equation 3.42.

3.5.0.4 Regular solution model

Thermodynamic properties of real solutions can be expressed in terms of their excess function, X^E [36]. The excess function is the difference between the observed thermodynamic function of mixing and the function for an ideal solution and is expressed in mathematical terms in Equation 3.44:

$$\Delta X^E = \Delta_{mix} X - \Delta_{mix} X^{ideal} \tag{3.44}$$

where X is the thermodynamic property, and $\Delta_{mix} X^{ideal}$ is given in Equation 3.34, 3.35 and 3.36 for G, H, and S, respectively. Since the ideal value for enthalpy of mixing is zero, the excess value must be equal to the observed enthalpy of mixing as shown in Equation 3.45.

$$\Delta H_m^E = \Delta_{mix} H_m \tag{3.45}$$

How much the excess energies deviate from zero indicates the extent to which the solution is non-ideal. To explain the non-ideal behaviour of a solution, the regular solution model is often used, which is a quantitative explanation. This model assumes the entropy of mixing is equal to the ideal entropy of mixing, meaning $\Delta S_m^E = 0$, but $\Delta H_m^E \neq 0$. According to the regular solution model, ΔH_m^E is dependent on the composition expressed by Equation 3.46 for a binary solution with component A and B.

$$\Delta H_m^E = \alpha R T x_A x_B \tag{3.46}$$

In Equation 3.46, α is a parameter that can be defined as a function of temperature according to Equation 3.47.

$$\alpha = \frac{\Omega}{RT} \tag{3.47}$$

For real solutions, the average A-B interactions can no longer be assumed to be the same as A-A and B-B interactions in a binary solution. In the regular solution

model, the Ω is an indication of the energy of A-B interactions relative to A-A and B-B, and by this model it is assumed to be constant. If $\Omega = 0$ we have an ideal solution, and if $\Omega < 0$ we have stabilisation of the solution, meaning A and B would mix rather than separate. If $\Omega > 0$, we have destabilisation, and A and B would separate rather than mix. The excess function of Gibbs energy for a regular solution can be found through the relation in Equation 3.1. Since $\Delta S_m^E = 0$, it follows that $\Delta G_m^E = \Delta H_m^E$ and the $\Delta_{mix} G_m$ for a binary solution with component A and B is expressed by Equation 3.48.

$$\begin{aligned} \Delta_{mix} G_m &= \Delta_{mix} G_m^E + \Delta_{mix} G_m^{ideal} \\ &= \Omega x_A x_B + \Delta_{mix} H_m^{ideal} - T \Delta_{mix} S_m^{ideal} \\ &= \Omega x_A x_B + 0 + RT(x_A ln x_A + x_B ln x_B) \end{aligned} \tag{3.48}$$

Then the total Gibbs energy of a binary solution with component A and B can be described according to Equation 3.49.

$$\begin{aligned} G &= G_m + \Delta_{mix} G_m \\ &= \mu_A^* x_A + \mu_B^* x_B + \Omega x_A x_B + RT(x_A ln x_A + x_B ln x_B) \end{aligned} \tag{3.49}$$

3.5.0.5 Sub-regular solution model

In the regular solution model, the interaction parameter, Ω, is constant. This indicates that the graph of Gibbs energy vs. mole fraction gives a symmetric curve [38]. However, for real alloy systems, this graph is usually asymmetric, and it is necessary to introduce a model with more than one free parameter. When the regular solution model is unable to reproduce the properties of a solution, the more convenient sub-regular solution model can be applied. It is a polynomial expression with more than two parameters, and the interaction parameter is no longer constant. Some approximations of the interaction parameter are suggested, but the most famous one is called the "Redlich-Kister polynomials" and will be used in this thesis. Therefore, only this approximation will be presented here, and $\Delta_{mix} G_m^E$ according to this model is shown in Equation 3.50.

$$\begin{aligned} &\Delta_{mix} G_m^E = x_A x_B [L(0) + L(1)(x_A - x_B) + L(2)(x_A - x_B)^2 + ... \\ &+ L(n)(x_A - x_B)^n] \end{aligned} \tag{3.50}$$

From Equation 3.50, the interaction parameter, Ω', for this version of the subregular solution model is defined as:

$$\Omega' = L(0) + L(1)(x_A - x_B) + L(2)(x_A - x_B)^2 + ... + L(n)(x_A - x_B)^n \quad (3.51)$$

$L(n)$ is a function of the temperature and is defined by Equation 3.52.

$$L(n) = a + bT \quad (3.52)$$

Here, a and b are constants and T is the temperature in K. For this approximation, the activity coefficient of component A in a binary system with component A and B, is given by Equation 3.53, and the derivation is shown in Appendix C.2

$$ln\gamma_A = \frac{1}{RT}[(1 - x_A)^2\Omega' + x_A x_B^2 \frac{d\Omega'}{dx_A}] \quad (3.53)$$

By replacing Ω with the Ω' in Equation 3.49, we get the total Gibbs energy of a binary system with component A and B, according to this version of the subregular solution model.

3.6 Transpiration method

Several different methods for vapour pressure measurements have been developed, and in this work, the transpiration method was used [39]. It is a dynamic method, which can be applied to both organic and inorganic compounds. It involves passing an inert carrier gas through a packed column with a sample of either the pure component or a mixture containing the component of interest. By measuring the weight change before and after the sample is exposed to the carrier gas, the apparent vapour pressure can be calculated. In the case where the sample is a mixture, the component of interest must be the most volatile one and the other components should have such low vapour pressure that their values can be neglected. There are several advantages of this method, such as the possibility to measure the vapour pressure within a short time in any atmosphere by changing the flow rate of the carrier gas, it is not influenced significantly by a small amount of volatile impurities, and it can be applied to temperatures that are close to ambient. The transpiration method has been proved to give results in agreement with other established techniques for vapour pressure determination, and, in principle, it is a

method free of significant errors.

In this thesis, the apparent vapour pressure of Bi, p_{Bi}, above the different samples were calculated using the weight change before and after an experiment for each sample. Bi will evaporate according to Equation 3.54 and Equation 3.55, and appear as Bi and Bi_2 in gas phase.

$$\mathrm{Bi\,(l)} \rightleftharpoons \mathrm{Bi\,(g)} \qquad (3.54) \qquad\qquad 2\,\mathrm{Bi\,(g)} \rightleftharpoons \mathrm{Bi_2(g)} \qquad (3.55)$$

In this work, Ar gas was used as carrier gas, and the calulcations were based on the assumptions that the only gases in the packed column, a quartz tube in our case, was Bi (g), Bi_2(g) and Ar (g). The calculations are carried out by deriving two expressions for the amount of moles of Bi as a function of the partial pressure of Bi. This was achieved by using the following equations:

$$p_{Bi} = \frac{n_{Bi}}{n_{Bi} + n_{Bi_2} + n_{Ar}} p_{tot} \tag{3.56}$$

where n_{Bi}, n_{Bi_2} and n_{Ar} are the number of moles of Bi, Bi_2 vapour and Ar gas, respectively, p_{tot} is the total pressure in the quartz tube (1 atm). The value of n_{Bi} was deduced by Equation 3.57:

$$\frac{\Delta W}{M_{Bi}} = n_{Bi} + n_{Bi_2} \tag{3.57}$$

where ΔW is weight change of Bi in grams caused by evaporation, M_{Bi} is the molar mass of Bi equal to 209 g/mol, n_{Bi} and n_{Bi_2} are the number of moles of Bi and Bi_2, respectively, in mol. The number of moles of the carrier gas, Ar, was deduced from Equation 3.58:

$$n_{Ar} = \frac{v_{Ar} t p_{Ar}}{R T_a} \tag{3.58}$$

where v_{Ar} is the argon flow rate in m^3/min, p_{Ar} is the pressure of Ar gas equal to 1.013×10^5 Pa, R is the gas constant equal to 8.314 J/Kmol, T_a is the temperature of the flow meter equal to 298 K, and t is the holding time of each sample in minutes. From the ideal gas law and the expression for Gibbs energy of reaction

3.55 (see Equation C.10 in Appendix C.1), we obtain the relation given in Equation 3.59:

$$\frac{n_{Bi_2}}{n_{Bi}} = \frac{p_{Bi_2}}{p_{Bi}} = p_{Bi} exp(\frac{\Delta G_2^0}{RT}) \tag{3.59}$$

where p_{Bi} and p_{Bi_2} are the partial vapour pressure in atm of Bi and Bi_2, respectively, R is the gas constant, and T is the experimental temperature in K. ΔG_2^0 is Gibbs energy of the reaction given in Equation 3.55, at the specific temperature T in J/mol.

By combining Equation 3.57 and Equation 3.59, the first expression for n_{Bi} is obtained and given in Equation 3.60.

$$n_{Bi} = \frac{\Delta W}{M_{Bi}(1 + 2(exp(\frac{\Delta G_2^0}{RT} p_{Bi}))} \tag{3.60}$$

The second expression is given in Equation 3.61, and obtained by combining Equation3.56, Equation 3.58 and Equation 3.59.

$$n_{Bi} = \frac{v_{Ar} t p_{Bi} p_{Ar}}{RT_a(p_{tot} - p_{Bi} - p_{Bi}^2 exp(\frac{\Delta G_2^0}{RT})} \tag{3.61}$$

The apparent vapour pressure of Bi from each sample was then obtained by putting Equation 3.60 and 3.61 equal to each other and solved graphically using Excel.

Chapter 4

Experimental

All experiments in this work have been carried out in Professor Uda's laboratory at Kyoto University, and all chemicals and tools used in this work are provided from his laboratory. Transpiration experiments were performed by the author of this thesis, and the preparation of the alloys was carried out in cooperation with PhD student Akihiro Kishimoto.

4.1 Experimental equipment

All vapour pressure experiments were carried out in a horizontal furnace, which is built around a sintered alumina tube, and heated by high power electric $MoSi_2$ heating elements. Figure 4.1 shows an illustration of the experimental setup, which consist of a 130 cm quartz tube placed in the alumina tube and a gas inlet and outlet through two rubber plugs. Quartz wool insulation was used to fill the gap between the quartz tube and the alumina tube to prevent heat loss. During all the experiments the furnace was kept at constant temperature, which was read at the sample position using a type K (chromel- alumel) thermocouple with an accuracy of ± 2.2°C. All chemicals and samples were weighed on an analytical scale with an estimated error of ± 0.1 mg.

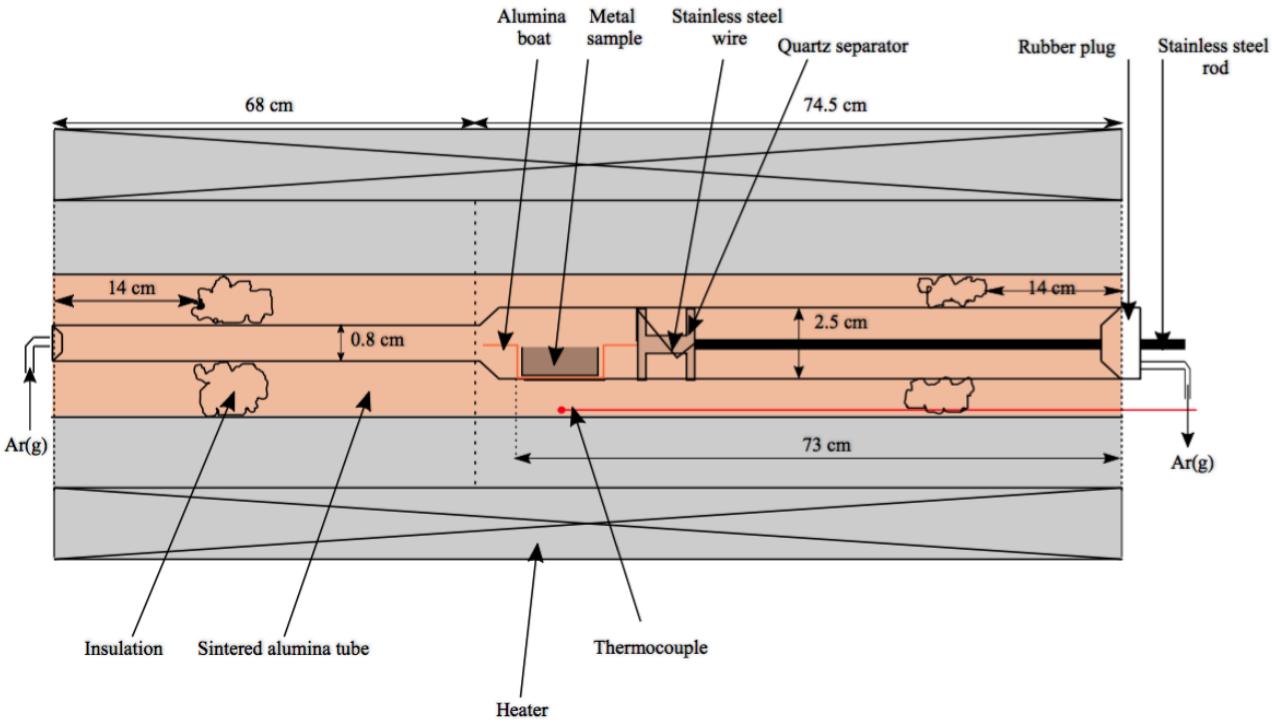

Figure 4.1: Schematic illustration of the experimental setup.

Ar gas was used as carrier gas, and the flow rate was controlled by a needle valve with a variable area flow meter (KOFLOC, RK1250) at the gas inlet and controlled by another flow meter (Agilent Technologies, ADM 1000) at the outlet with an accuracy of ±2% and ±3%, respectively. During experiments, the flow rates were measured by indications of O_2 gas and H_2 gas and converted to the correct argon gas flow rates for calculations. The conversion calculation is presented in Appendix A.1, and further, on the correct Ar gas flow rates are used. Each sample with pure Bi and Bi−Ti alloys were placed in a Mo-foil boat, which again was placed in an alumina boat. The Bi−Sn alloys were placed directly in an alumina boat. Figure 4.2 and Figure 4.3 illustrate an alumina boat and Mo-foil boat, respectively.

Figure 4.2: A picture of an alumina boat.

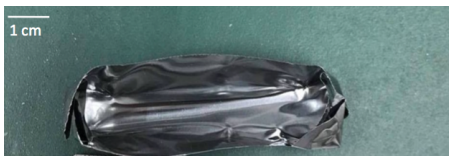

Figure 4.3: A picture of a Mo-foil boat.

A device for inserting the alumina boat to the middle of the quartz tube was also developed, and a picture is presented in Figure 4.4. The device consists of a quartz separator connected to a stainless steel rod, and a rubber plug with two stainless steel tubes, one for the gas outlet and one for a stainless steel rod used to insert the sample. As can be seen in Figure 4.4, an ultra torr, a tool connecting the stainless steel tube and the stainless steel rod, was used for vacuum connections that can be opened and closed as desired. When the ultra torr is locked, the stainless steel rod is rigid, and when it is open, the stainless steel rod is movable. The ultra torr also sealed the gap between the stainless steel tube and stainless steel rod so no air would enter the quartz tube.

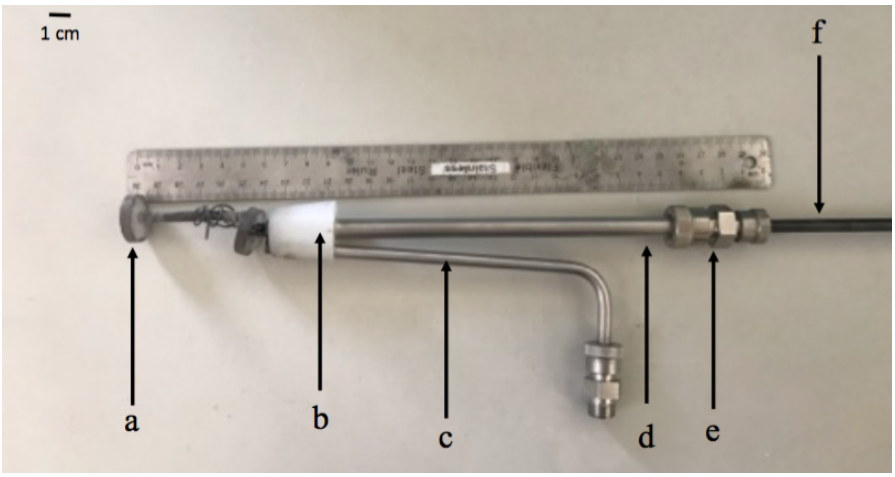

Figure 4.4: The inserting device for inserting sample in the quartz tube. a) quartz separator, b) rubber plug, c) stainless steel tube for gas outlet, d) stainless steel tube e) ultra torr and f) stainless steel rod.

4.2 Preparation of alloys/samples

A large batch of pure bismuth spheres was prepared by leaching in 1 M nitric acid to remove the outer oxidation layer, dried for two days in a vacuum dryer, and stored in a glove box filled with Ar gas (with an oxygen concentration < 0.1ppm) for later use. The prepared Bi was used to make alloys and for experiments with pure Bi. A list of the metals used is given in Table 4.1, together with their purity grade and manufacturer.

Bi−Ti alloys

Bi and Ti were mixed with certain compositions, and placed in MgO crucibles. The MgO cruicbles were placed in stainless steel containers, together with a Mo-foil filled with Ti sponge to prevent the mixtures from oxidising. A stainless steel lid was placed on top of each container and sealed with tape in a glove box. Then the containers were moved from the glove box and sealed by TIG welding. To form homogeneous alloys, the stainless steel containers containing the MgO crucibles with the metal mixture were placed in a vertical furnace at a temperature of 1000° for 40 hours. After 40 hours, the containers were quenched in water at room temperature, opened, and the alloys were separated from the MgO crucibles by use of different working tools, such as hammer and chisel. Two different Bi−Ti alloys, Bi−30 mol% Ti and Bi−40 mol% Ti, were prepared and the various mixing compositions are presented in Table 4.2. The alloys were stored in a glove box with Ar gas when not in use to prevent Ti from reacting with moisture and air.

Bi−Sn alloys

The Sn−Bi alloys were made using the experimental setup shown in Figure 4.1, under Ar gas flow rate of 179 dm^3/min. Bi and Sn powder with the certain compositions were mixed in an alumina boat and connected to the stainless steel rod (see Figure 4.4). The alumina boat was inserted 10 cm into the quartz tube, where the temperature was 200°C and kept at this position until the mixture had melted. The furnace was then evacuated and refilled with Ar gas alternately three times, and the flow rate was adjusted. Then the alumina boat, containing the mixture, was inserted into the middle of the quartz tube where the temperature was 900°C with a holding time of one hour. After one hour, the alumina boat was repositioned to the end of the quartz tube and kept at this position until the alloy had solidified. Two different Bi−Sn alloys, Bi−50 mol% Sn and Bi−70 mol% Sn, were prepared and the various compositions are presented in Table 4.2.

Table 4.1: List of metals used with their purity grade and manufacturer.

Metal	Grade & manufacturer
Bi	99.99%, Kamioka Mining & Smelting co., Ltd.
Ti	>99.0%, Wako Pure Chemical Industries, Ltd.
Sn	99.9%, Kojund Chemical Laboratory Co., Ltd

Table 4.2: Compositions of the metals required to make the specific alloys.

Alloy	Total weight of sample [g]	Bi [g]	Ti [g]	Sn[g]
Bi	20	20.00	0.000	0.000
Bi – 30 mol%Ti	40	36.42	3.575	0.000
Bi – 40 mol%Ti	40	34.71	5.290	0.000
Bi – 50 mol%Sn	20	12.76	0.000	7.240
Bi – 70 mol%Sn	20	8.600	0.000	11.40

4.3 The experimental procedure

The alumina boat, which contained the sample and alternatively Mo-foil, was weighed and connected to the quartz separator, which in turn was attached to the stainless steel rod. The alumina boat was then inserted into the opening of the quartz tube. The quartz tube was evacuated, removing air and moisture, before refilling it with Ar gas. This process was repeated four times before each experiment, and the desired gas flow rate was then adjusted accordingly. The alumina boat was inserted into the middle of the quartz tube, where the desired temperature was obtained, and kept there with a holding time of two hours. After two hours, the sample was repositioned to the end of the quartz tube and maintained at this position until the sample solidified. This typically lasted approximately 30 minutes, and the sample was then weighed.

Experiments with samples of pure Bi, Bi – 30 mol% Ti alloy, Bi – 40 mol% Ti alloy at 900°C were carried out, and additionally, a few experiments with pure Bi at 800°C. Control experiments with Bi – 50 mol% Sn alloy and Bi – 70 mol% Sn alloy were also performed to ensure the experimental equipment was properly functioning. The changes in weight and related gas flow rates for each experiment can be found in Table A.1-A.6 in Appendix A.2. The holding time for each experiment was two hours, except one experiment with pure Bi at 800°C which had a holding time of 15 hours.

Chapter 5

Results

The following chapter presents the results of the experimental work. The apparent vapour pressure of Bi above each sample was calculated using the method described in Section 3.6, and the numerical values, together with their calculated standard error, are presented in Table B.1-B.6 in Appendix B. The calculation of the literature values can be seen in Appendix C.

Bi−Ti alloys at 900°C

Figure 5.1 and Figure 5.2 illustrate the apparent vapour pressure of Bi as a function of Ar gas flow rate, above the samples of Bi−30 mol% Ti and Bi−40 mol% Ti at 900°C. The apparent vapour pressure of Bi above pure Bi is also included in both figures. The dashed horizontal lines represent the calculated vapour pressure of Bi from literature values above their respective samples at 900°C.

From Figure 5.1 and Figure 5.2 it is evident that the apparent vapour pressure of Bi above the pure Bi follows a trend. For Ar gas flow rates less than 0.026 85 dm^3/min an apparent increase is observed, and for Ar gas flow rates higher than 0.134 25 dm^3/min a decrease is observed. However, the values plateau for Ar gas flow rates between 0.026 85 dm^3/min and 0.134 25 dm^3/min, showing almost independent behaviour with the gas flow rate. The experimental values of this observed plateau are in agreement with the literature value of 4.66×10^{-4} atm.

From Figure 5.1 and Figure 5.2, the values for Bi−30 mol% Ti alloy and Bi−40 mol% Ti alloy, are showing large variation. In the case of Bi−30 mol% Ti alloy the results vary between 3.7×10^{-4} atm and 4.9×10^{-4} atm, and only one measurement is in agreement with the calculated literature value of 3.66×10^{-4} atm. However, for

Bi−40 mol% Ti alloy the values vary between 3.7×10^{-4} atm and 6.3×10^{-4} atm, which is higher than the literature value of 3.05×10^{-4} atm. The average results from measurements of Bi−Ti alloy and pure Bi are plotted in Figure 5.3, together with their calculated standard error. The results show a slightly similar trend for both alloys, with increased apparent vapour pressure values at lower flow rates.

Additionally, the different activities for each measurement was calculated (see Table B.7-B.10 Appendix in B.1). The values for Bi−30 mol% Ti ranged from 0.79399 to 1.05150, with an average value of 0.91273. For Bi−40 mol% Ti, the values ranged from 0.79399 to 1.35193, with an average value of 0.93616.

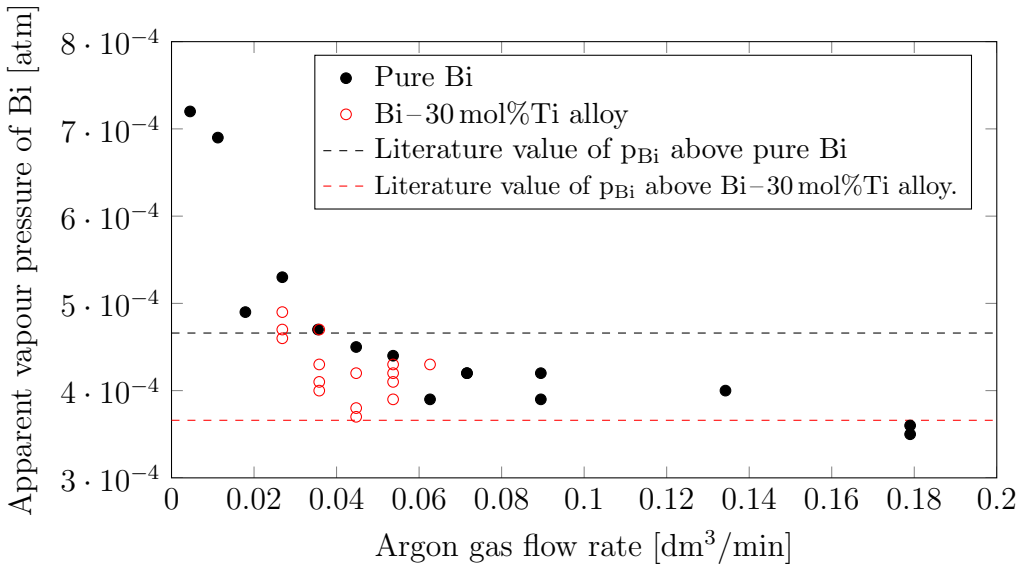

Figure 5.1: The apparent vapour pressure of Bi at 900°C as a function of Ar gas flow rate, with a holding time of 2 hours, above Bi−30 mol% Ti alloy, together with the literature values for each sample at this temperature.

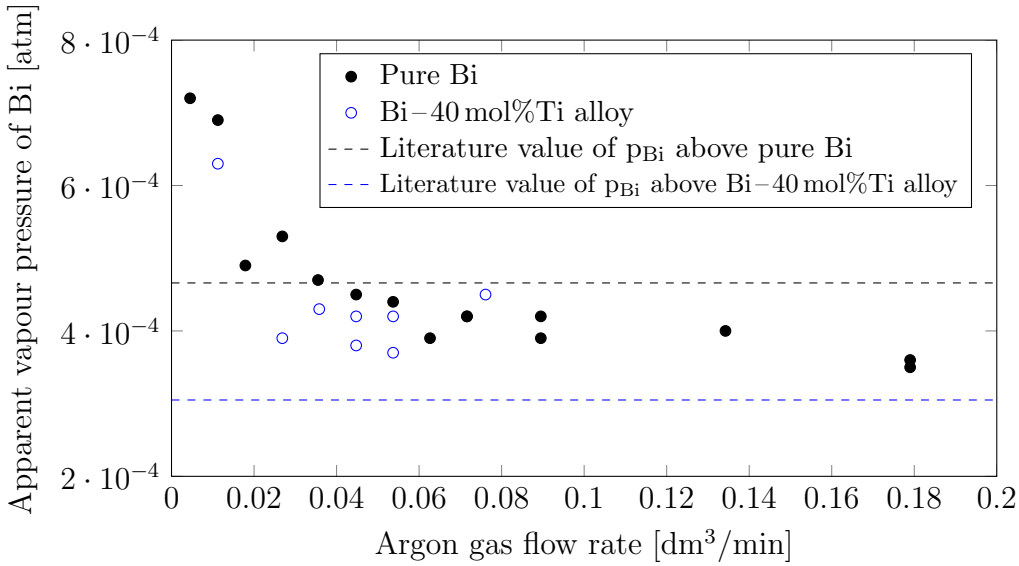

Figure 5.2: The apparent vapour pressure of Bi at 900°C as a function of Ar gas flow rate, with a holding time of 2 hours, above Bi−40 mol%Ti alloy, together with the literature values for each sample at this temperature.

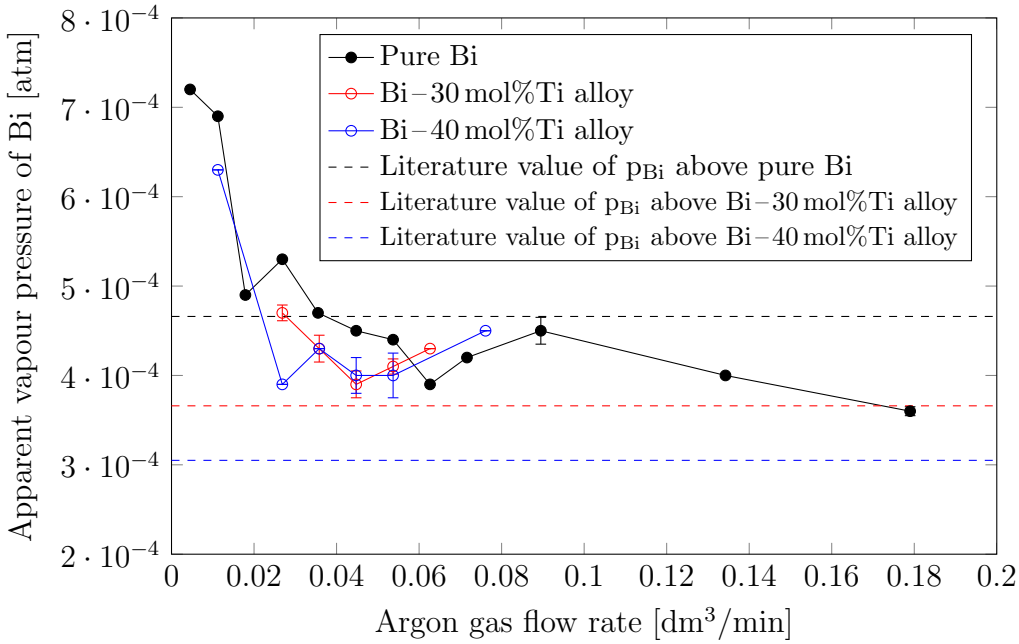

Figure 5.3: The average apparent vapour pressure of Bi at 900°C as a function of Ar gas flow rate, with a holding time of 2 hours, above Bi−Ti alloys, together with the literature values for each sample at this temperature.

Control experiments Bi−Sn alloys at 900°C

Figure 5.4 illustrates the apparent vapour pressure of Bi as a function of Ar gas flow rate, above the samples Bi−50 mol%Sn and Bi−70 mol%Sn at 900°C, together with the apparent vapour pressure of Bi above the pure Bi sample. The dashed horizontal lines represent the calculated vapour pressure of Bi from literature values over their respective samples at 900°C.

From Figure 5.4 it is evident that the apparent vapour pressure of Bi above Bi−50 mol%Sn and Bi−70 mol%Sn is consistent with their respective literature values, and they show almost an independent behaviour of the Ar flow rates. Additionally, the different activities for each measurement was calculated (see Table B.9-B.10 Appendix in B.1). The values for Bi−50 mol% Sn ranged from 0.40772 to 0.57940 with an average value of 0.53380. For Bi−70 mol% Sn, the values ranged from 0.21459 to 0.36481, with an average value of 0.29736.

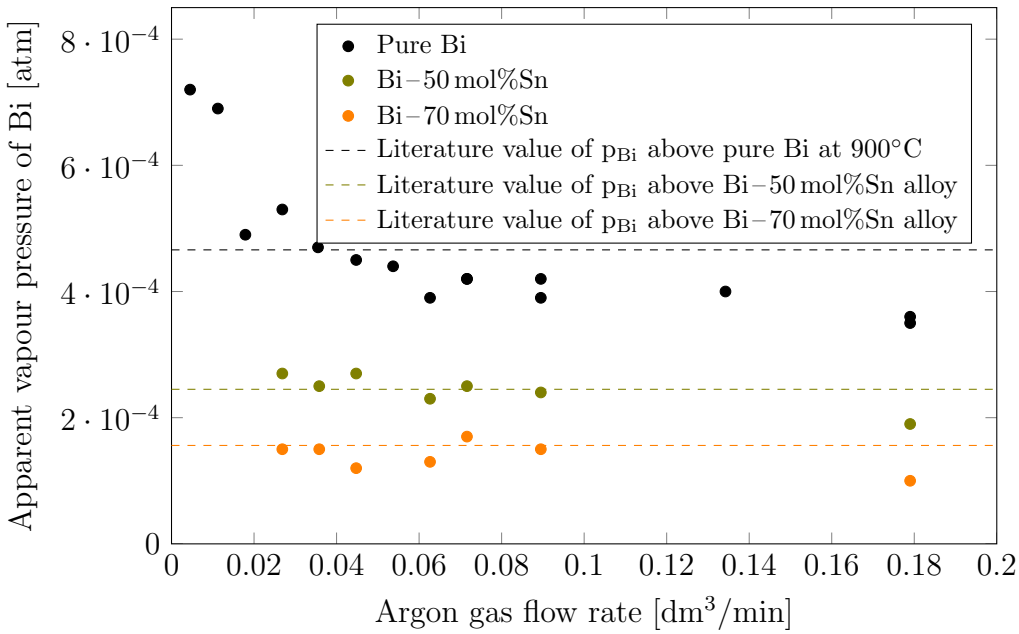

Figure 5.4: The apparent vapour pressure of Bi at 900°C as a function of Ar gas flow rate, with a holding time of 2 hours, above Bi−Sn alloys, together with the literature values for each sample at this temperature.

Pure Bi at 800°C

Figure 5.5 illustrates the apparent vapour pressure of Bi above pure Bi as a function of Ar gas flow rate at 800°C. The horizontal dashed line is the calculated vapour pressure of Bi above pure Bi from literature values at 800°C. The black points represent a holding time of 2 hours, while the grey point represents a holding time of 15 hours. Although the number of measurements is limited, leading to considerable variation in apparent vapour pressure values, no trend can be observed given the present data.

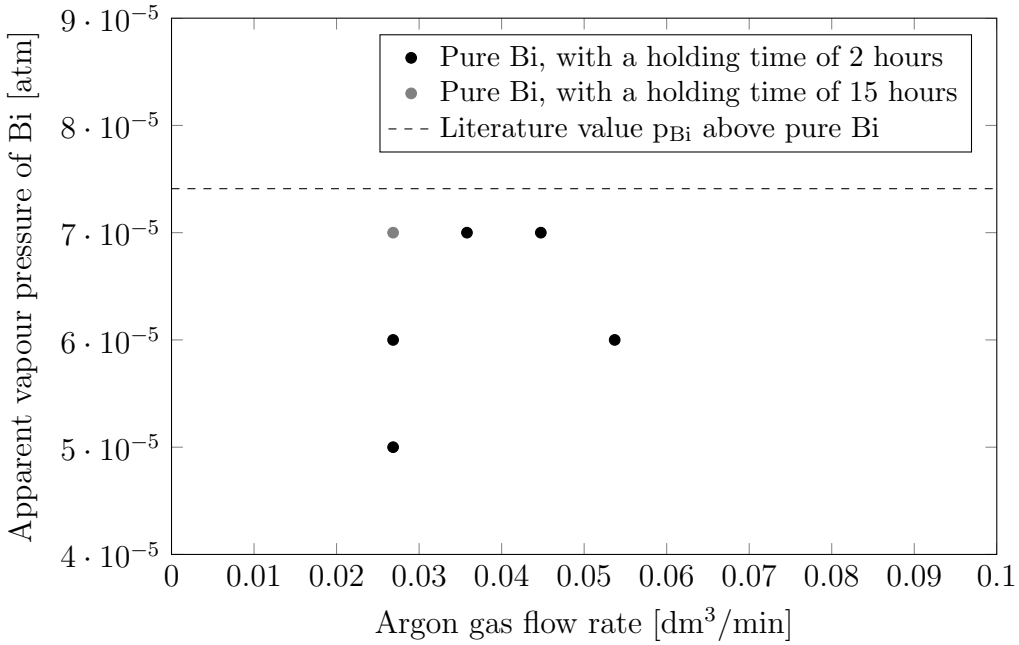

Figure 5.5: The apparent vapour pressure of Bi at 800°C as a function of Ar gas flow rate, with a holding time of 2 hours and 15 hours, above pure Bi, together with the literature value at this temperature.

Chapter 6

Discussion

When measuring the vapour pressure by the transpiration method described in Section 3.6, it is important that the component of interest is the dominant product of evaporation at the particular temperature. In our case, this means that the total product of evaporation originates from Bi. Therefore, the vapour pressures of pure Ti and pure Sn were calculated at 900°C (see Appendix C), and were determined to be 3.61×10^{-14} atm and 1.58×10^{-8} atm, respectively. Comparing these values with the calculated vapour pressure of Bi, 4.66×10^{-4} atm, it is clear that the difference is sufficiently large. It is therefore reasonable to assume that pure Ti and pure Sn will not have a severe effect, with the dominant product of evaporation originating from Bi.

It was assumed that the apparent vapour pressure was independent of the gas flow rate at equilibrium. By measuring the variation of the apparent vapour pressure of pure Bi, with the variation of Ar gas flow rate, the conditions were determined to be in the observed plateau region in Figure 5.1 and Figure 5.2 (0.026 85 dm^3/min to 0.134 25 dm^3/min).

Bi−Ti alloys at 900°C

Huang *et al.* [40] carried out thermodynamic modelling of the Bi−Ti system based on experimental data from previous literature and their work. They determined the parameters for calculating the interaction parameter, Ω', which were used to calculate the vapour pressure of Bi above Bi−Ti alloys at 900°C (see Appendix C.3). The literature value for Bi−30 mol% Ti and Bi−40 mol% Ti was determined to be 3.66×10^{-4} atm and 3.05×10^{-4} atm, respectively, and the empirical values

were expected to fall within the observed plateau region. From Figure 5.1 and Figure 5.2, it is evident that the apparent vapour pressure for Bi−30 mol% Ti and Bi−40 mol% Ti does not show the expected results. There is considerable variation in the apparent vapour pressure for both the alloys, and Figure 5.3 illustrates that the results have a higher value than expected. It is hard to distinguish the measurements from each alloy and pure Bi, as the measurements from the alloys are very similar to those for pure Bi.

One possible explanation can be that the Bi−Ti alloys were contaminated by the MgO crucible during alloy preparation, meaning that Bi reacted with the MgO to form Bi−Mg alloys instead of Bi−Ti alloys. In this case the Ti would have reacted with oxygen and forming TiO_2. Therefore, a control analysis was carried out on the Bi−30 mol% Ti alloy after vapour pressure measurements, by EPMA (JEOL, JXA-8530F). The results of the analysis can be seen in Appendix B.2, and the average composition of the alloy was determined to be 28 at.%Ti, which is in agreement with the nominal composition. However, the EDX spectrum (see Figure B.1) shows that no significant amount of magnesium was found in the alloy, meaning that Bi−Mg formations unlikely explained the unexpected results. EDX can not detect oxygen in the alloy, meaning there is still a possibility of oxygen contamination. Additionally, the Ti could have reacted with oxygen in the air during weighing, as this was carried out in the air. In the case of oxygen contamination, the Ti in the alloys would have formed the protective TiO_2 layer on the sample surface, alongside other Ti−O compounds. The oxygen would have added an artificial mass, giving a smaller weight change. Consequently, this gives a lower value for the apparent vapour pressure of Bi, such that it can not explain the high values obtained.

Throughout all the experiments, the same alloys were used, and the composition in the alloys changed for every measurement and may therefore explain the unexpected results. The total weight change of Bi−30 mol% Ti alloy was 0.995 g, and for Bi−40 mol% Ti 0.5379 g. Assuming the weight change was only due to evaporated Bi, this is equal to 0.6mol% change and 0.4mol% change of Bi−30 mol% Ti and Bi−40 mol% Ti, respectively. Consequently, the Ti concentration is increasing for each experiment, which should have resulted in lower apparent vapour pressure values of Bi, than expected. Based on this, a more significant difference between the results of the two alloys, and the results of pure Bi should be observed. Therefore, this is unlikely the cause of the too high vapour pressures observed, with the change being so small that the values can be neglected.

A further possibility is that liquid metal was spilled during repositioning of the alumina boat from the middle of the quartz tube to the opening, as the stainless steel rod is sensitive to rotation. In this case, a higher weight change would have been measured, resulting in greater measure vapour pressure for Bi. However, no metal was observed in the quartz tube after measurements, meaning that this explanation does not account for the high values observed.

The calculated literature value for the activity of Bi was determined to be 0.78724 and 0.65553 for Bi−30 mol% Ti and Bi−40 mol% Ti, respectively. By comparing these values with the average activity of the empirical results, it indicates that the real activity of Bi in Bi−Ti alloys is higher than predicted by the thermodynamic model suggested by Huang *et al.* [40]. If this is the case, it will explain the higher values for p_{Bi} in the Bi−Ti alloys obtained. However, as the thermodynamic properties of the Bi−Ti system have never been experimentally investigated before, more research is required in order to determine whether the activity of Bi is indeed higher than predicted.

Additionally, the unexpected values could have the simple explanation that the transpiration method can not be applied to this system, such that vapour pressure measurements of the Bi−Ti system should be carried out using another method. Given the results in this work, this seems like a reasonable explanation.

Assuming the results of this work are reliable, this would be beneficial for vacuum distillation in the alternative proposed process by Kado *et al.* [1], due to a higher apparent vapour pressure of Bi in Bi−Ti alloys than predicted from literature values. A higher content of Bi will therefore evaporate upon vacuum distillation than first predicted at the same temperature. However, for the magnesiothermic reduction step of $TiCl_4$, a low vapour pressure is desired to obtain the Bi in liquid phase.

Control experiments Bi-Sn alloys

To verify that the lack of any clear differences in the apparent vapour pressure of Bi−Ti alloys was not due to a faulty experimental setup, control experiments with Bi−Sn alloys were performed. The Bi−Sn system was chosen because Sn has such low vapour pressure, and therefore is unlikely affecting the calculations on Bi. Additionally, the thermodynamic properties of this system have been experimentally investigated in previous literature [41]. From Figure 5.4 we see that

the results are in agreement with the calculated literature values for the vapour pressure above both of the alloys tested. They also show an almost independent behaviour of the apparent vapour pressure to the Ar gas flow rate, falling into the expected region with plateau behaviour. The calculated literature values for the activities of Bi in the Bi−Sn alloys was determined to be 0.52631 and 0.33519 for Bi−50 mol% Sn and Bi−70 mol% Sn, respectively. Comparing these with the average empirical activity values for each alloy, we see a slight difference corresponding to the difference between the measured vapour pressure of Bi and the calculated vapour pressure. It is therefore unlikely that the experimental setup can account for the unexpected results in the Bi−Ti system.

Pure Bi at 800°C

The results from these measurements showed very small values for the pressure. However, given the poor accuracy, it was concluded that the experimental error was too large. The measurements at this temperature are therefore not included.

Chapter 7

Future Work

The experiments should be repeated in a non-oxygen atmosphere. For instance, the end of the quartz tube could be connected to a glove box under argon atmosphere, and the samples weighed before and after experiments in the same glove box. This is to decrease the possibility of the Ti in the alloys to react with oxygen.

The vapour pressure of Bi above Bi−Ti alloys was not successfully measured by the transpiration method, and vapour pressure measurements should be repeated by a different experimental method. For instance, the Knudsen Cell method could be applied, which involves determining the vapour pressure from the evaporation rate.

Chapter 8

Conclusions

The aim of this work was to examine the operating conditions for a new titanium production route (Kado *et al.* [1]) by empirically investigating the thermodynamic properties of the Bi−Ti system. Specifically, the apparent vapour pressure of Bi above samples of pure Bi, Bi−30 mol% Ti alloy, and Bi−40 mol% Ti alloy was measured by the transpiration method at 900°C. However, the present results suggest that it is not possible to measure the vapour pressure of Bi above Bi−Ti alloys by the transpiration method. This is possibly due to Ti in the Bi−Ti alloys reacting with oxygen, or the activity of Bi in these alloys being slightly higher than calculated based on previous literature. The average activity of Bi−30 % Ti was found to be 0.91273, and 0.93616 for Bi−40 mol% Ti, which is higher than the calculated activity based on previous literature. For Bi−Sn alloys the average activiy was determined to be 0.53380 and 0.29736 for Bi−50 mol% Sn and Bi−70 mol% Sn, respectively. Consequently, the proper operating conditions of vacuum distillation, segregation, and the reaction heat by reduction of $TiCl_4$ by Mg could not be precisely calculated.

References

[1] Y. Kado, A. Kishimoto, and T. Uda, "New smelting process for titanium: magnesiothermic reduction of ticl4 into liquid bi and subsequent refining by vacuum distillation," *Metallurgical and Materials Transactions B*, vol. 46, no. 1, pp. 57–61, 2015.

[2] C. A. Hampel, "Encyclopedia of the chemical elements," 1968.

[3] S. J. Gerdemann, "Titanium process technologies," *Advanced materials & processes*, vol. 159, no. DOE/ARC-2002-007, 2001.

[4] H. Åsheim, "Cathodic deposition of titanium in chloride melts," Master's thesis, NTNU, 10 2010.

[5] M. J. Donachie, *Titanium: a technical guide*. ASM international, 2000.

[6] T. B. Company, "Aero – boeing 787 from the ground up." `http://www.boeing.com/commercial/aeromagazine/articles/qtr_4_06/article_04_2.html`, 2017. Accessed: 2017-04-18.

[7] A. Hauge, "titan." `https://sml.snl.no/titan`, 2017. Accessed: 2017-04-18.

[8] C. R. Nagesh, C. Ramachandran, and R. Subramanyam, "Methods of titanium sponge production," *Transactions of the Indian Institute of Metals*, vol. 61, no. 5, pp. 341–348, 2008.

[9] M. Ma, D. Wang, W. Wang, X. Hu, X. Jin, and G. Z. Chen, "Extraction of titanium from different titania precursors by the ffc cambridge process," *Journal of Alloys and Compounds*, vol. 420, no. 1, pp. 37–45, 2006.

[10] U. MetalMiner, "Titanium, metalminerprices." `https://agmetalminer.com/metal-prices/titanium/`, 2017. Accessed: 2017-04-27.

[11] G. Z. Chen, D. J. Fray, and T. W. Farthing, "Direct electrochemical reduction of titanium dioxide to titanium in molten calcium chloride," *Nature*, vol. 407, no. 6802, pp. 361–364, 2000.

[12] D. Whittaker, "Swot testing for pm titanium at prague gathering," *Metal Powder Report*, vol. 61, no. 1, pp. 8–12, 2006.

[13] L. Woodruff and G. Bedinger, "Titanium-light,strong, and white." `https://pubs.usgs.gov/fs/2013/3059/`, 2017. Accessed: 2017-05-01.

[14] M. E. Weeks, "The discovery of the elements. xi. some elements isolated with the aid of potassium and sodium: Zirconium, titanium, cerium, and thorium," *J. Chem. Educ*, vol. 9, no. 7, p. 1231, 1932.

[15] M. A. Hunter, "Metallic titanium.," *Journal of the American Chemical Society*, vol. 32, no. 3, pp. 330–336, 1910.

[16] S. R. Seagle, "Titanium processing." `https://global.britannica.com/technology/titanium-processing#toc81523`, 2017. Accessed: 2017-05-03.

[17] S. Hutchison, C. Wai, J. Dong, and R. Kearney, "Titanium production in a plasma reactor: a feasibility investigation," *Plasma Chemistry and Plasma Processing*, vol. 15, no. 2, pp. 353–367, 1995.

[18] F. Yang and V. Hlavacek, "Recycling titanium from ti-waste by a low-temperature extraction process," *AIChE journal*, vol. 46, no. 12, pp. 2499–2503, 2000.

[19] O. S. Kjos, "Electrochemical production of titanium by using titanium oxycarbide anodes in molten salts," 2010.

[20] R. Subramanyam, "Some recent innovations in the kroll process of titanium sponge production," *Bulletin of Materials Science*, vol. 16, no. 6, pp. 433–451, 1993.

[21] G. H. Aylward and T. J. V. Findlay, *SI chemical data*. Australia, John Wiley, 6 ed., 2008.

[22] G. M. Haarberg, "Magnesium smelter technology," in *Encyclopedia of Applied Electrochemistry*, pp. 1210–1213, Springer, 2014.

[23] G. M. Haarberg, "Electrochemical behaviour of dissolved titanium oxides during aluminium deposition from molten fluoride electrolytes," *Materials transactions*, vol. 58, no. 3, pp. 406–409, 2017.

[24] M. Ginnata, G. Orsello, R. Berruti, M. Gaido, and E. Serra, "Industrial plant for the production of electrolytic titanium," 1988.

[25] G. Z. Chen and D. J. Fray, "Understanding the electro-reduction of metal oxides in molten salts," in *LIGHT METALS-WARRENDALE-PROCEEDINGS-*, pp. 881–886, TMS, 2004.

[26] C. Schwandt, G. R. Doughty, and D. J. Fray, "The ffc-cambridge process for titanium metal winning," in *Key Engineering Materials*, vol. 436, pp. 13–25, Trans Tech Publ, 2010.

[27] K. Ono and R. O. Suzuki, "A new concept for producing ti sponge: calciothermic reduction," *JOM Journal of the Minerals, Metals and Materials Society*, vol. 54, no. 2, pp. 59–61, 2002.

[28] T. H. Okabe, T. Oda, and Y. Mitsuda, "Titanium powder production by preform reduction process (prp)," *Journal of Alloys and Compounds*, vol. 364, no. 1, pp. 156–163, 2004.

[29] M. V. Ginatta, G. Orsello, and R. Berruti, "Method and cell for the electrolytic production of a polyvalent metal," May 1991. US Patent 5.015.342.

[30] M. V. Ginatta, 1986. European Patent 0.210.961.

[31] Y. Kado, A. Kishimoto, and T. Uda, "Electrolysis of tio2 or ticl2 using bi liquid cathode in molten cacl2," *Journal of The Electrochemical Society*, vol. 160, no. 10, pp. E139–E142, 2013.

[32] A. Kishimoto, Y. Kado, and T. Uda, "Electrorefining of titanium from bi–ti alloys in molten chlorides for a new smelting process of titanium," *Journal of Applied Electrochemistry*, vol. 46, no. 9, pp. 987–993, 2016.

[33] P. Q. James and W. G. Wilfrid, "Electrolytic manufacture of titanium," July 31 1956. US Patent 2,757,135.

[34] S. Maruyama, Y. Kado, and T. Uda, "Phase diagram investigations of the bi-ti system," *Journal of Phase Equilibria and Diffusion*, vol. 34, no. 4, pp. 289–296, 2013.

[35] G. Vassilev, X. Liu, and K. Ishida, "Reaction kinetics and phase diagram studies in the ti–zn system," *Journal of alloys and compounds*, vol. 375, no. 1, pp. 162–170, 2004.

[36] P. Atkins and J. de Paula, *Atkins' Physical Chemistry.* Oxford University Press, 2002.

[37] D. R. Gaskell, *Introduction to the Thermodynamics of Materials.* CRC Press, 2008.

[38] S. Stølen and T. Grande, *Chemical thermodynamics of materials: macroscopic and microscopic aspects.* John Wiley & Sons, 2004.

[39] S. P. Verevkin and V. N. Emel'yanenko, "Transpiration method: Vapor pressures and enthalpies of vaporization of some low-boiling esters," *Fluid Phase Equilibria*, vol. 266, no. 1, pp. 64–75, 2008.

[40] L. Huang, Q. Chen, Y. He, X. Tao, G. Cai, H. Liu, and Z. Jin, "Thermodynamic modeling of fe–ti–bi system assisted with key experiments," *Calphad*, vol. 46, pp. 34–41, 2014.

[41] J. Vizdal, M. H. Braga, A. Kroupa, K. W. Richter, D. Soares, L. F. Malheiros, and J. Ferreira, "Thermodynamic assessment of the bi–sn–zn system," *Calphad*, vol. 31, no. 4, pp. 438–448, 2007.

[42] L. Fluid Industry Co., "Technical data gas volume 1-1.." `http://www.ryutai.co.jp/shiryou/gas/gas-01.htm`, 2017. Accessed: 2017-01-26.

[43] I. Barin and G. Platzki, *Thermochemical data of pure substances*. VCH, New York, 3 ed., 1995.

Appendix A

Experimental

A.1 Conversion of flow meter values

To convert O_2 gas and H_2 gas flow meter values to correct Ar gas values, Equation A.1 and Equation A.2 were used. Q_{O_2} [dm^3/min] is the indicated value on the O_2 flow meter, Q_{H_2} [dm^3/min] is the indicated value on H_2 flow meter, and Q_{Ar} [dm^3/min] is the corrected Ar gas value.

$$Q_{Ar} = Q_{H_2}\sqrt{\frac{\rho_{H_2}}{\rho_{Ar}}} = Q_{H2} \cdot 0.2245 \tag{A.1}$$

$$Q_{Ar} = Q_{O_2}\sqrt{\frac{\rho_{O_2}}{\rho_{Ar}}} = Q_{O2} \cdot 0.8950 \tag{A.2}$$

Where ρ_{H_2}, ρ_{O_2}, and ρ_{Ar} are densities at 298 K and 1 atm pressure for H_2, O_2, and Ar, respectively, and taken from reference [42].

$\rho_{H_2} = 0.0824\,\mathrm{kg/m^3}$
$\rho_{O_2} = 1.3092\,\mathrm{kg/m^3}$
$\rho_{Ar} = 1.6343\,\mathrm{kg/m^3}$

A.2 Experimental data

The different weight losses for each sample are presented in Table A.1-A.6 together with their respective Ar gas flow rates, temperature, and holding time.

Table A.1: Weight losses, ΔW, at Ar gas flow rate, v_{Ar}, and temperature, T, with holding time, t, for pure Bi.

Sample	T [K]	t [min]	v_{Ar} [dm^3/min]	ΔW [g]
Pure Bi	1173	120	0.17900	0.2040
Pure Bi	1173	120	0.17900	0.2121
Pure Bi	1173	120	0.13425	0.1879
Pure Bi	1173	120	0.08950	0.1206
Pure Bi	1173	120	0.08950	0.1345
Pure Bi	1173	120	0.07160	0.1128
Pure Bi	1173	120	0.07160	0.1133
Pure Bi	1173	120	0.06265	0.0858
Pure Bi	1173	120	0.05370	0.0903
Pure Bi	1173	120	0.04475	0.0768
Pure Bi	1173	120	0.03550	0.0683
Pure Bi	1173	120	0.02685	0.0632
Pure Bi	1173	120	0.01790	0.0368
Pure Bi	1173	120	0.01123	0.0406
Pure Bi	1173	120	0.00450	0.0183

Table A.2: Weight losses, ΔW, at Ar gas flow rate, v_{Ar}, and temperature, T, with holding time, t, for Bi−30 mol% Ti alloy.

Sample	T [K]	t [min]	v_{Ar} [dm^3/min]	ΔW [g]
Bi−30 mol% Ti alloy	1173	120	0.06265	0.1028
Bi−30 mol% Ti alloy	1173	120	0.05370	0.0870
Bi−30 mol% Ti alloy	1173	120	0.05370	0.0833
Bi−30 mol% Ti alloy	1173	120	0.05370	0.0795
Bi−30 mol% Ti alloy	1173	120	0.05370	0.0738
Bi−30 mol% Ti alloy	1173	120	0.04475	0.0557
Bi−30 mol% Ti alloy	1173	120	0.04475	0.0689
Bi−30 mol% Ti alloy	1173	120	0.04475	0.0579
Bi−30 mol% Ti alloy	1173	120	0.03580	0.0537
Bi−30 mol% Ti alloy	1173	120	0.03580	0.0684
Bi−30 mol% Ti alloy	1173	120	0.03580	0.0535
Bi−30 mol% Ti alloy	1173	120	0.03580	0.0575
Bi−30 mol% Ti alloy	1173	120	0.02685	0.0485
Bi−30 mol% Ti alloy	1173	120	0.02685	0.0495
Bi−30 mol% Ti alloy	1173	120	0.02685	0.0551

Table A.3: Weight losses, ΔW, at Ar gas flow rate, v_{Ar}, and temperature, T, with holding time, t for Bi−40 mol% Ti alloy.

Sample	T [K]	t [min]	v_{Ar} [dm^3/min]	ΔW [g]
Bi−40 mol% Ti alloy	1173	120	0.07610	0.1236
Bi−40 mol% Ti alloy	1173	120	0.05370	0.0848
Bi−40 mol% Ti alloy	1173	120	0.05370	0.0688
Bi−40 mol% Ti alloy	1173	120	0.04475	0.0586
Bi−40 mol% Ti alloy	1173	120	0.04475	0.0708
Bi−40 mol% Ti alloy	1173	120	0.03580	0.0568
Bi−40 mol% Ti alloy	1173	120	0.02685	0.0389
Bi−40 mol% Ti alloy	1173	120	0.01123	0.0356

Table A.4: Weight losses, ΔW, at Ar gas flow rate, v_{Ar}, and temperature, T, with holding time, t, Bi−50 mol% Sn alloy.

Sample	T [K]	t [min]	v_{Ar} [dm^3/min]	ΔW [g]
Bi−50 mol% Sn alloy	1173	120	0.17900	0.0768
Bi−50 mol% Sn alloy	1173	120	0.08950	0.0554
Bi−50 mol% Sn alloy	1173	120	0.07160	0.0479
Bi−50 mol% Sn alloy	1173	120	0.06265	0.0357
Bi−50 mol% Sn alloy	1173	120	0.04475	0.0333
Bi−50 mol% Sn alloy	1173	120	0.03580	0.0226
Bi−50 mol% Sn alloy	1173	120	0.02685	0.0201

Table A.5: Weight losses, ΔW, at Ar gas flow rate, v_{Ar}, and temperature, T, with holding time, t, for Bi−50 mol% Sn alloy.

Sample	T [K]	t [min]	v_{Ar} [dm^3/min]	ΔW [g]
Bi−70 mol% Sn alloy	1173	120	0.17900	0.0472
Bi−70 mol% Sn alloy	1173	120	0.08950	0.0274
Bi−70 mol% Sn alloy	1173	120	0.07160	0.0256
Bi−70 mol% Sn alloy	1173	120	0.06265	0.0144
Bi−70 mol% Sn alloy	1173	120	0.04475	0.0093
Bi−70 mol% Sn alloy	1173	120	0.03580	0.0107
Bi−70 mol% Sn alloy	1173	120	0.02685	0.0078

Table A.6: Weight losses, ΔW, at Ar gas flow rate, v_{Ar}, and temperature, T, with holding time, t, for pure Bi.

Sample	T [K]	t [min]	v_{Ar} [dm^3/min]	ΔW [g]
Pure Bi	1073	120	0.05370	0.0155
Pure Bi	1073	120	0.04475	0.0178
Pure Bi	1073	120	0.03580	0.0127
Pure Bi	1073	120	0.02685	0.0082
Pure Bi	1073	120	0.02685	0.0060
Pure Bi	1073	900	0.02685	0.0688

Appendix B

Results

The apparent vapour pressure for each sample was calculated according to the method described in Section 3.6, using the weight losses in Table A.1-A.6. The values are presented in Table B.1-B.6, together with their respective Ar gas flow rates, temperature, holding time and standard error. The standard error for the results with several measurements for each flow rate is calculated according to the method described in Appendix C.3.0.1.

Table B.1: The apparent vapour pressure of Bi, p_{Bi}, at Ar gas flow rate, v_{Ar}, and temperature, T, with holding time, t, above pure Bi.

Sample	T [K]	t [min]	v_{Ar} [dm^3/min]	p_{Bi} [atm]	Standard error
Pure Bi	1173	120	0.17900	3.5×10^{-4}	5.0×10^{-6}
Pure Bi	1173	120	0.17900	3.6×10^{-4}	
Pure Bi	1173	120	0.13425	4.0×10^{-4}	
Pure Bi	1173	120	0.08950	3.9×10^{-4}	1.5×10^{-5}
Pure Bi	1173	120	0.08950	4.2×10^{-4}	
Pure Bi	1173	120	0.07160	4.2×10^{-4}	
Pure Bi	1173	120	0.07160	4.2×10^{-4}	
Pure Bi	1173	120	0.06265	3.9×10^{-4}	
Pure Bi	1173	120	0.05370	4.4×10^{-4}	
Pure Bi	1173	120	0.04475	4.5×10^{-4}	
Pure Bi	1173	120	0.03550	4.7×10^{-4}	
Pure Bi	1173	120	0.02685	5.3×10^{-4}	
Pure Bi	1173	120	0.01790	4.9×10^{-4}	
Pure Bi	1173	120	0.01123	6.9×10^{-4}	
Pure Bi	1173	120	0.00450	7.2×10^{-4}	

Table B.2: The apparent vapour pressure of Bi, p_{Bi}, at Ar gas flow rate, v_{Ar}, and temperature, T, with holding time, t, above pure Bi−30 mol% Ti alloy.

Sample	T [K]	t [min]	v_{Ar} [dm^3/min]	p_{Bi} [atm]	Standard erreor
Bi−30 mol% Ti alloy	1173	120	0.06265	4.3×10^{-4}	
Bi−30 mol% Ti alloy	1173	120	0.05370	4.3×10^{-4}	8.5×10^{-6}
Bi−30 mol% Ti alloy	1173	120	0.05370	4.2×10^{-4}	
Bi−30 mol% Ti alloy	1173	120	0.05370	4.1×10^{-4}	
Bi−30 mol% Ti alloy	1173	120	0.05370	3.9×10^{-4}	
Bi−30 mol% Ti alloy	1173	120	0.04475	3.7×10^{-4}	1.5×10^{-5}
Bi−30 mol% Ti alloy	1173	120	0.04475	4.2×10^{-4}	
Bi−30 mol% Ti alloy	1173	120	0.04475	3.8×10^{-4}	
Bi−30 mol% Ti alloy	1173	120	0.03580	4.0×10^{-4}	1.5×10^{-5}
Bi−30 mol% Ti alloy	1173	120	0.03580	4.7×10^{-4}	
Bi−30 mol% Ti alloy	1173	120	0.03580	4.1×10^{-4}	
Bi−30 mol% Ti alloy	1173	120	0.03580	4.3×10^{-4}	
Bi−30 mol% Ti alloy	1173	120	0.02685	4.6×10^{-4}	8.8×10^{-6}
Bi−30 mol% Ti alloy	1173	120	0.02685	4.7×10^{-4}	
Bi−30 mol% Ti alloy	1173	120	0.02685	4.9×10^{-4}	

Table B.3: The apparent vapour pressure of Bi, p_{Bi}, at Ar gas flow rate, v_{Ar}, and temperature, T, with holding time, t, above Bi−40 mol% Ti alloy.

Sample	T [K]	t [min]	v_{Ar} [dm^3/min]	p_{Bi} [atm]	Standard error
Bi−40 mol% Ti alloy	1173	120	0.07610	4.5×10^{-4}	
Bi−40 mol% Ti alloy	1173	120	0.05370	4.2×10^{-4}	2.5×10^{-4}
Bi−40 mol% Ti alloy	1173	120	0.05370	3.7×10^{-4}	
Bi−40 mol% Ti alloy	1173	120	0.04475	3.8×10^{-4}	2.0×10^{-4}
Bi−40 mol% Ti alloy	1173	120	0.04475	4.2×10^{-4}	
Bi−40 mol% Ti alloy	1173	120	0.03580	4.3×10^{-4}	
Bi−40 mol% Ti alloy	1173	120	0.02685	3.9×10^{-4}	
Bi−40 mol% Ti alloy	1173	120	0.01123	6.3×10^{-4}	

Table B.4: The apparent vapour pressure of Bi, p_{Bi}, at Ar gas flow rate, v_{Ar}, and temperature, T, with holding time, t, above Bi−50 mol% Sni alloy.

Sample	T [K]	t [min]	v_{Ar} [dm^3/min]	p_{Bi} [atm]
Bi−50 mol% Sn alloy	1173	120	0.17900	1.9×10^{-4}
Bi−50 mol% Sn alloy	1173	120	0.08950	2.4×10^{-4}
Bi−50 mol% Sn alloy	1173	120	0.07160	2.5×10^{-4}
Bi−50 mol% Sn alloy	1173	120	0.06265	2.3×10^{-4}
Bi−50 mol% Sn alloy	1173	120	0.04475	2.7×10^{-4}
Bi−50 mol% Sn alloy	1173	120	0.03580	2.5×10^{-4}
Bi−50 mol% Sn alloy	1173	120	0.02685	2.7×10^{-4}

Table B.5: The apparent vapour pressure of Bi, p_{Bi}, at Ar gas flow rate, v_{Ar}, and temperature,T, with holding time, t, above Bi−70 mol% Sni alloy.

Sample	T [K]	t [min]	v_{Ar} [dm^3/min]	p_{Bi} [atm]
Bi−70 mol% Sn alloy	1173	120	0.17900	1.0×10^{-4}
Bi−70 mol% Sn alloy	1173	120	0.08950	1.5×10^{-4}
Bi−70 mol% Sn alloy	1173	120	0.07160	1.7×10^{-4}
Bi−70 mol% Sn alloy	1173	120	0.06265	1.3×10^{-4}
Bi−70 mol% Sn alloy	1173	120	0.04475	1.2×10^{-4}
Bi−70 mol% Sn alloy	1173	120	0.03580	1.5×10^{-4}
Bi−70 mol% Sn alloy	1173	120	0.02685	1.5×10^{-4}

Table B.6: The apparent vapour pressure of Bi, p_{Bi}, at Ar gas flow rate, v_{Ar}, and temperature, T, with holding time, t, above pure Bi.

Sample	T [K]	t [min]	v_{Ar} [dm^3/min]	p_{Bi} [atm]
Pure Bi	1073	120	0.05370	6.0×10^{-5}
Pure Bi	1073	120	0.04475	7.0×10^{-5}
Pure Bi	1073	120	0.03580	7.0×10^{-5}
Pure Bi	1073	120	0.02685	6.0×10^{-5}
Pure Bi	1073	120	0.02685	5.0×10^{-5}
Pure Bi	1073	900	0.02685	7.0×10^{-5}

B.1 Calculated activity of Bi in Bi−Ti and Bi−Sn alloys

The activities of Bi in the Bi-Ti alloys and Bi-Sn alloys were calculated according to Equation 3.42 in Section 3.5.0.3, where $p^*_{Bi} = 4.66 \times 10^{-4}$ atm.The values are presented in Table B.7-B.10.

Table B.7: The apparent vapour pressure of Bi, p_{Bi}, at Ar gas flow rate, v_{Ar}, and temperature, T, with holding time, t, and the calculated activity of Bi, a_{Bi}, above Bi−30 mol% Ti.

Sample	T [K]	t [min]	v_{Ar} [dm^3/min]	p_{Bi} [atm]	a_{Bi}
Bi−30 mol% Ti alloy	1173	120	0.06265	4.3×10^{-4}	0.92275
Bi−30 mol% Ti alloy	1173	120	0.05370	4.3×10^{-4}	0.92275
Bi−30 mol% Ti alloy	1173	120	0.05370	4.2×10^{-4}	0.90128
Bi−30 mol% Ti alloy	1173	120	0.05370	4.1×10^{-4}	0.87983
Bi−30 mol% Ti alloy	1173	120	0.05370	3.9×10^{-4}	0.83691
Bi−30 mol% Ti alloy	1173	120	0.04475	3.7×10^{-4}	0.79399
Bi−30 mol% Ti alloy	1173	120	0.04475	4.2×10^{-4}	0.90128
Bi−30 mol% Ti alloy	1173	120	0.04475	3.8×10^{-4}	0.81545
Bi−30 mol% Ti alloy	1173	120	0.03580	4.0×10^{-4}	0.85837
Bi−30 mol% Ti alloy	1173	120	0.03580	4.7×10^{-4}	1.00858
Bi−30 mol% Ti alloy	1173	120	0.03580	4.1×10^{-4}	0.87983
Bi−30 mol% Ti alloy	1173	120	0.03580	4.3×10^{-4}	0.92275
Bi−30 mol% Ti alloy	1173	120	0.02685	4.6×10^{-4}	0.98712
Bi−30 mol% Ti alloy	1173	120	0.02685	4.7×10^{-4}	1.00858
Bi−30 mol% Ti alloy	1173	120	0.02685	4.9×10^{-4}	1.05150

Table B.8: The apparent vapour pressure of Bi, p_{Bi}, at Ar gas flow rate, v_{Ar}, and temperature, T, with holding time, t, and the calculated activity of Bi, a_{Bi}, above Bi−40 mol% Ti.

Sample	T [K]	t [min]	v_{Ar} [dm^3/min]	p_{Bi} [atm]	a_{Bi}
Bi−40 mol% Ti alloy	1173	120	0.07610	4.5×10^{-4}	0.96566
Bi−40 mol% Ti alloy	1173	120	0.05370	4.2×10^{-4}	0.90129
Bi−40 mol% Ti alloy	1173	120	0.05370	3.7×10^{-4}	0.79399
Bi−40 mol% Ti alloy	1173	120	0.04475	3.8×10^{-4}	0.81545
Bi−40 mol% Ti alloy	1173	120	0.04475	4.2×10^{-4}	0.90129
Bi−40 mol% Ti alloy	1173	120	0.03580	4.3×10^{-4}	0.92275
Bi−40 mol% Ti alloy	1173	120	0.02685	3.9×10^{-4}	0.83691
Bi−40 mol% Ti alloy	1173	120	0.01123	6.3×10^{-4}	1.35193

Table B.9: The apparent vapour pressure of Bi, p_{Bi}, at Ar gas flow rate, v_{Ar}, and temperature, T, with holding time, t, and the calculated activity of Bi, a_{Bi}, above Bi−50 mol% Sn.

Sample	T [K]	t [min]	v_{Ar} [dm^3/min]	p_{Bi} [atm]	a_{Bi}
Bi−50 mol% Sn alloy	1173	120	0.17900	1.9×10^{-4}	0.40772
Bi−50 mol% Sn alloy	1173	120	0.08950	2.4×10^{-4}	0.51502
Bi−50 mol% Sn alloy	1173	120	0.07160	2.5×10^{-4}	0.53648
Bi−50 mol% Sn alloy	1173	120	0.06265	2.3×10^{-4}	0.49356
Bi−50 mol% Sn alloy	1173	120	0.04475	2.7×10^{-4}	0.57939
Bi−50 mol% Sn alloy	1173	120	0.03580	2.5×10^{-4}	0.53648
Bi−50 mol% Sn alloy	1173	120	0.02685	2.7×10^{-4}	0.57940

Table B.10: The apparent vapour pressure of Bi, p_{Bi}, at Ar gas flow rate, v_{Ar}, and temperature, T, with holding time, t, and the calculated activity of Bi, a_{Bi}, above Bi−70 mol% Sn.

Sample	T [K]	t [min]	v_{Ar} [dm^3/min]	p_{Bi} [atm]	a_{Bi}
Bi−70 mol% Sn alloy	1173	120	0.17900	1.0×10^{-4}	0.21459
Bi−70 mol% Sn alloy	1173	120	0.08950	1.5×10^{-4}	0.32189
Bi−70 mol% Sn alloy	1173	120	0.07160	1.7×10^{-4}	0.36481
Bi−70 mol% Sn alloy	1173	120	0.06265	1.3×10^{-4}	0.27897
Bi−70 mol% Sn alloy	1173	120	0.04475	1.2×10^{-4}	0.25751
Bi−70 mol% Sn alloy	1173	120	0.03580	1.5×10^{-4}	0.32189
Bi−70 mol% Sn alloy	1173	120	0.02685	1.5×10^{-4}	0.32189

B.2 EDX analysis of Bi−30 mol% Ti

The area analysed of the Bi−30 mol% Ti is given in Figure B.1a. The avarage composition is presented in Table B.11 and Figure B.1 is showing the EDX spectrum of the area analysed in the Bi−30 mol% Ti alloy.

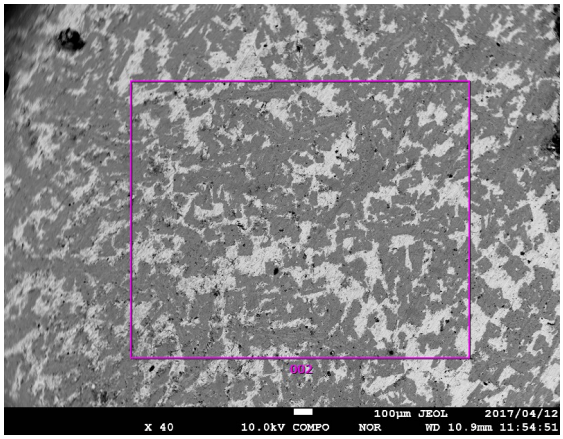

(a)

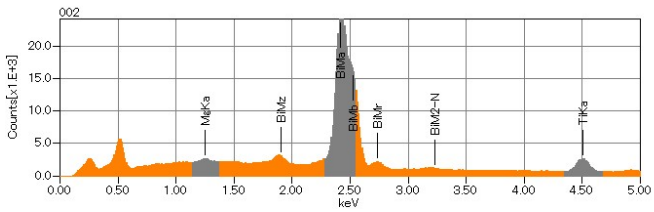

(b)

Figure B.1: a) Back-scattered SEM image of Bi−30 mol% Ti after vapour pressure measurements. b) EDX spectrum of the area analysed, X-rays from K and M shell.

Table B.11: EDX analysis data.

Element	wt.%	at.%
Ti	8.22	28.10
Bi	91.78	71.90
Sum	100.00	100.00

Appendix C

Calculations

C.1 Calculated partial vapour pressure from literature values

Partial vapour pressure of pure Bi at 1173 K and 1073 K

When bismuth evaporates, it reacts according to the chemical reactions given in Equation C.1 and Equation C.2.

$$\mathrm{Bi\,(l)} \rightleftharpoons \mathrm{Bi\,(g)} \qquad \text{(C.1)} \qquad\qquad 2\,\mathrm{Bi\,(g)} \rightleftharpoons \mathrm{Bi_2(g)} \qquad \text{(C.2)}$$

At equilibrium, their Gibbs energy values are equal and can be expressed as in Equation C.3 and Equation C.4.

$$\Delta G^0_{Bi(l)} = \Delta G^0_{Bi(g)} \qquad \text{(C.3)} \qquad\qquad 2\Delta G^0_{Bi(g)} = \Delta G^0_{Bi_2(g)} \qquad \text{(C.4)}$$

Consequently, will Equation C.5 and Equation C.6 also be true, and by rearranging these two equations, the Gibbs energy for the two reactions in Equation C.1 and Equation C.2 can be expressed as in Equation C.7 and Equation C.8, respectively.

$$G^0_{Bi(l)} + RTlna_{Bi(l)} = G^0_{Bi(g)} + RTlnp_{Bi(g)} \tag{C.5}$$

$$2G^0_{Bi(g)} + 2RTlnp_{Bi(g)} = G^0_{Bi(g)} + RTlnp_{Bi_2(g)} \tag{C.6}$$

$$\begin{aligned}\Delta G^0_1 &= G^0_{Bi(l)} - G^0_{Bi(g)} \\ &= RTlnp_{Bi(g)} - RTlna_{Bi(l)} \\ &= RTln\frac{p_{Bi(g)}}{a_{Bi(l)}}\end{aligned} \tag{C.7}$$

$$\begin{aligned}\Delta G^0_2 &= 2G^0_{Bi(g)} - G^0_{Bi_2(g)} \\ &= RTlnp^2_{Bi(g)} - RTlnp_{Bi_2(g)} \\ &= RTln\frac{p^2_{Bi(g)}}{p_{Bi_2(g)}}\end{aligned} \tag{C.8}$$

Knowing the activity, a, is equal to 1 for pure substances, and solving Equation C.7 and Equation C.8 with respect to $p_{Bi(g)}$ and $p_{Bi_2(g)}$, respectively, two new expressions for the vapour pressure are obtained as shown in Equation C.9 and Equation C.10.

$$p_{Bi(g)} = exp(\frac{\Delta G^0_1}{RT}) \tag{C.9}$$

$$p_{Bi_2(g)} = exp(\frac{\Delta G^0_2}{RT}) \cdot p^2_{Bi(g)} \tag{C.10}$$

Where ΔG^0_1 and ΔG^0_2 were calculated in Equation C.11 and Equation C.12, using the values below from reference [43].

$G^0_{Bi(l)}$ at 1173 K = −91.744 20 kJ/mol
$G^0_{Bi(g)}$ at 1173 K = −24.973 11 kJ/mol
$G^0_{Bi_2(g)}$ at 1173 K = −128.275 73 kJ/mol

$$\begin{aligned}\Delta G^0_1 &= G^0_{Bi(l)} - G^0_{Bi(g)} \\ &= -99774.20 + 24973.11 \\ &= -74\,801.09\ \text{J/mol}\end{aligned} \tag{C.11}$$

$$\begin{aligned}\Delta G^0_2 &= 2G^0_{Bi(g)} - G^0_{Bi_2(g)} \\ &= 2(-24973.11) + 128275.73 \\ &= 78\,329.51\ \text{J/mol}\end{aligned} \tag{C.12}$$

The partial vapour pressure of Bi and Bi_2 are calculated in Equation C.13 and Equation C.14, respectively, and the total vapour pressure contributing from Bi is calculated in Equation C.15.

$$p_{Bi(g)} = exp(\frac{-74801.09}{8.314 \cdot 1173}) = 4.66 \times 10^{-4}\,\text{atm} \tag{C.13}$$

$$p_{Bi_2(g)} = exp(\frac{78329.51}{8.314 \cdot 1173})(4.66 \times 10^{-4})^2 = 6.68 \times 10^{-4}\,\text{atm} \tag{C.14}$$

$$p_{tot} = p_{Bi} + 2p_{Bi_2} = 1.802 \times 10^{-3}\,\text{atm} \tag{C.15}$$

The partial vapour pressure of Bi at 1073 K was calculated in the same way, and the values for $G^0_{Bi(l)}$, $G^0_{Bi(g)}$ and $G^0_{Bi_2(l)}$ at 1073 K are taken from reference [43], giving a literature value of Bi, $p_{Bi} = 7.41 \times 10^{-5}$ atm.

Partial vapour pressure of pure Ti at 1173 K

The partial vapour pressure of Ti was calculated in the same way as for Bi, but with a different initially chemical equation, and only the calculation is shown in this part.

$$\text{Ti(s)} \rightleftharpoons \text{Ti(g)} \tag{C.16}$$

$$\Delta G^0_{Ti(s)} = \Delta G^0_{Ti(g)} \tag{C.17}$$

$$G^0_{Ti(s)} + RTlna_{Ti(s)} = G^0_{Ti(g)} + RTlnp_{Ti(g)} \tag{C.18}$$

$$\begin{aligned} \Delta G^0_3 &= G^0_{Ti(s)} - G^0_{Ti(g)} \\ &= RTlnp_{Ti(g)} - RTlna_{Ti(s)} \\ &= RTln\frac{p_{Ti(g)}}{a_{Ti(s)}} \end{aligned} \tag{C.19}$$

$$p_{Ti(g)} = exp(\frac{\Delta G^0_3}{RT}) \tag{C.20}$$

Values taken from reference [43]:
$G^0_{Ti(s)}$ at 1173 K $= -56.306\,50$ kJ/mol

$G^0_{Ti(g)}$ at 1173 K = 245.564 18 kJ/mol

$$\begin{aligned}\Delta G^0_3 &= G^0_{Ti(s)} - G^0_{Ti(g)} \\ &= -56306.50 - 245564.18 \\ &= -301\,870.68\,\mathrm{J/mol}\end{aligned} \tag{C.21}$$

$$p_{Ti(g)} = exp(\frac{-301870.68}{8.314 \cdot 1173}) = 3.61 \times 10^{-14}\,\mathrm{atm} \tag{C.22}$$

Partial vapour pressure of pure Sn at 1173 K

The partial vapour pressure of Sn was calculated in the same way as for Bi, but with a different initially chemical, and only the calculation is shown in this part.

$$\mathrm{Sn\,(l)} \rightleftharpoons \mathrm{Sn\,(g)} \tag{C.23}$$

$$\Delta G^0_{Sn(l)} = \Delta G^0_{Sn(g)} \tag{C.24}$$

$$G^0_{Sn(l)} + RTlna_{Sn(l)} = G^0_{Sn(g)} + RTlnp_{Sn(g)} \tag{C.25}$$

$$\begin{aligned}\Delta G^0_4 &= G^0_{Sn(l)} - G^0_{Sn(g)} \\ &= RTlnp_{Sn(g)} - RTlna_{Sn()} \\ &= RTln\frac{p_{Sn(g)}}{a_{Sn(l)}}\end{aligned} \tag{C.26}$$

$$p_{Sn(g)} = exp(\frac{\Delta G^0_4}{RT}) \tag{C.27}$$

Values taken from reference [43]:
$G^0_{Sn(l)}$ at 1173 K = −90.355 40 kJ/mol
$G^0_{Sn(g)}$ at 1173 K = 84.795 47 kJ/mol

$$\begin{aligned}\Delta G_3^0 &= G_{Sn(l)}^0 - G_{Sn(g)}^0 \\ &= -90355.40 - 84795.47 \\ &= -175\,150.87\,\mathrm{J/mol}\end{aligned} \tag{C.28}$$

$$p_{Sn(g)} = exp(\frac{-175150.87}{8.314 \cdot 1173}) = 1.58 \times 10^{-8}\,\mathrm{atm} \tag{C.29}$$

C.2 Deriving the activity coefficient for sub-regular solution model

In this section the expression for the activity coefficient, γ_A, given in Equation 3.53, will be derived for a binary solution containing components A and B according to the sub-regular solution model. Equation C.30 and Equation C.31 are used to derive γ_A:

$$\mu_A = G + x_B \frac{dG}{dx_A} \tag{C.30}$$

$$G = \mu_A^* x_A + \mu_B^* x_B + \Omega' x_A x_B + RT(x_A lnx_A + x_B lnx_B) \tag{C.31}$$

where Ω' is given in Equation C.32.

$$\begin{aligned}\Omega' &= L(0) + L(1)(x_A - x_B) + L(2)(x_A - x_B)^2 + ... + L(n)(x_A - x_B)^n \\ &= L(0) + L(1)(2x_A - 1) + L(2)(2x_A - 1)^2 + ... + L(n)(2x_A - 1)^n\end{aligned} \tag{C.32}$$

Using $x_A + x_B = 1$, the term $\frac{dG}{dx_A}$ from Equation C.30 is derived as shown in Equation C.33.

$$\begin{aligned}\frac{dG}{dx_A} &= \frac{d(\mu_A^* x_A + \mu_B^* x_B + RT(x_A lnx_A + x_B lnx_B) + \Omega' x_A x_B)}{dx_A} \\ &= \mu_A^* - \mu_B^* + RT(lnx_A - lnx_B) + (1 - 2x_A)\Omega' + x_A x_B \frac{d\Omega'}{dx_A}\end{aligned} \tag{C.33}$$

By putting C.31 and C.33 into C.30, Equation C.34 is obtained.

$$\begin{aligned}\mu_A &= \mu_A^* x_A + \mu_B^* x_B + \Omega' x_A x_B + RT(x_A ln x_A + x_B ln x_B) \\ &+ x_B(\mu_A^* - \mu_B^* + RT(ln x_A - ln x_B) + (1-2x_A)\Omega' + x_A x_B \frac{d\Omega'}{dx_A}) \\ &= \mu_A^* + RT ln x_A + x_A x_B^2 \frac{d\Omega'}{dx_A} + \Omega'(1-x_A)^2\end{aligned} \tag{C.34}$$

By rearranging Equation C.34 to Equation C.35, putting Equation C.35 equal to Equation C.36, and solving for $ln\gamma_A$, the desired expression given in Equation C.37 is obtained.

$$\mu_A - \mu_A^* = RT ln x_A + x_A x_B^2 \frac{d\Omega'}{dx_A} + \Omega'(1-x_A)^2 \tag{C.35}$$

$$\mu_A - \mu_A^* = RT ln a_A = RT ln x_A \gamma_A = RT(ln x_A + ln\gamma_A) \tag{C.36}$$

$$ln\gamma_A = \frac{1}{RT}[(1-x_A)^2\Omega' + x_A x_B^2 \frac{d\Omega'}{dx_A}] \tag{C.37}$$

C.3 Vapour pressure of Bi over Bi−Ti and Bi−Sn alloys

Bi−Ti alloys

Huang *et al.* [40] determined the thermodynamic parameters of the Bi−Ti system based on experimental data from previous literature and their own work. They defined the thermodynamic parameters $L(0)$, $L(1)$, and $L(2)$ for this system to be:

$$L(0) = -43216.537 + 26.975T \tag{C.38}$$

$$L(1) = 43171.650 - 27.757T \tag{C.39}$$

$$L(2) = -1836.172 + 5.028T \tag{C.40}$$

where $L(0)$, $L(1)$, and $L(2)$ are given in J/mol, and T is the temperature in K. In this work, these definitions are applied to the sub-regular solution model to calculate the literature values for the vapour pressure of Bi above Bi−Ti alloys at 1173 K, as presented below.

Bi−30 mol% Ti alloy

Ω' and $\frac{d\Omega'}{dx_{Bi}}$ are obtained at 1173 K, for Bi−30 mol%Ti alloy, meaning $x_Bi = 0.7$, as shown in Equation C.41 and Equation C.42.

$$\begin{aligned}\Omega' &= L(0) + L(1)(2x_{Bi} - 1) + L(2)(2x_{Bi} - 1)^2 \\ &= -43216.537 + 26.975(1173) + (43171.650 - 27.757(1173))(2 \cdot 0.7 - 1) \\ &+ (-1836.172 + 5.028(1173))(2 \cdot 0.7 - 1)^2 \\ &= -6679.92\end{aligned} \tag{C.41}$$

$$\begin{aligned}\frac{d\Omega'}{dx_{Bi}} &= 2L(1) + 4L(2)(2x_{Bi} - 1) \\ &= 2(43171.650 - 27.757T) + 4(-1836.172 + 5.028(1173))(2 \cdot 0.7 - 1) \\ &= 27724.05\end{aligned} \tag{C.42}$$

By putting Equation C.41 and C.42 into Equation C.37, and calculating the numerical value, where R is the gas constant in J/Kmol and T is the temperature in K, Equation C.43 is obtained.

$$\begin{aligned}ln\gamma_{Bi} &= \frac{1}{RT}[(1 - x_{Bi})^2\Omega' + x_{Bi}x_{Ti}^2\frac{d\Omega'}{dx_{Bi}}] \\ &= \frac{1}{8.314 \cdot 1173}[(1 - 0.7)^2 \cdot (-65679.92) + 0.7 \cdot 0.3^2(27724.05)] \\ &= 0.11745\end{aligned} \tag{C.43}$$

Equation C.43 is solved with respect to γ_{Bi} and the literature partial vapour pressure value is calculated as shown in Equation C.44 to C.46.

$$\gamma_{Bi} = exp(0.11745) = 1.12463 \tag{C.44}$$

$$a_{Bi} = x_{Bi}\gamma_{Bi} = 1.12463 \cdot 0.7 = 0.78724 \tag{C.45}$$

$$p_{Bi} = a_{Bi}p^*_{Bi} = 0.78724 \cdot 4.66 \times 10^{-4} = 3.66 \times 10^{-4}\,\text{atm} \tag{C.46}$$

Bi−40 mol% Ti alloy

Ω' and $\frac{d\Omega'}{dx_{Bi}}$ are obtained at 1173 K, for Bi−40 mol% Ti alloy, meaning $x_Bi = 0.6$, as shown in Equation C.47 and Equation C.48.

$$\begin{aligned}\Omega' &= L(0) + L(1)(2x_{Bi} - 1) + L(2)(2x_{Bi} - 1)^2 \\ &= -43216.537 + 26.975(1173) + (43171.650 - 27.757(1173))(2 \cdot 0.6 - 1) \\ &+ (-1836.172 + 5.028(1173))(2 \cdot 0.6 - 1)^2 \\ &= -9289.86\end{aligned} \tag{C.47}$$

$$\begin{aligned}\frac{d\Omega'}{dx_{Bi}} &= 2L(1) + 4L(2)(2x_{Bi} - 1) \\ &= 2(43171.650 - 27.757(1173)) + 4(-1836.172 + 5.028(1173))(2 \cdot 0.6 - 1) \\ &= 24474.72\end{aligned} \tag{C.48}$$

By putting Equation C.47 and C.48 into Equation C.37, and calculating the numerical value, where R is the gas constant in J/Kmol and T is the temperature in K, Equation C.49 is obtained.

$$\begin{aligned}ln\gamma_{Bi} &= \frac{1}{RT}[(1 - x_{Bi})^2\Omega' + x_{Bi}x_{Ti}^2\frac{d\Omega'}{dx_{Bi}}] \\ &= \frac{1}{8.314 \cdot 1173}[(1 - 0.6)^2 \cdot (-9289.86) + 0.6 \cdot 0.4^2(24474.72)] \\ &= 0.08851\end{aligned} \tag{C.49}$$

Equation C.49 is solved with respect to γ_{Bi} and the literature partial vapour pressure value is calculated as shown in Equation C.50 to C.52.

$$\gamma_{Bi} = exp(0.08851) = 1.09255 \tag{C.50}$$

$$a_{Bi} = x_{Bi}\gamma_{Bi} = 1.09255 \cdot 0.6 = 0.65553 \tag{C.51}$$

$$p_{Bi} = a_{Bi}p^*_{Bi} = 0.65553 \cdot 4.66 \times 10^{-4} = 3.05 \times 10^{-4}\,\text{atm} \tag{C.52}$$

Bi−Sn alloys

Vizdal *et al.* [41] carried out a thermodynamic assessment of the Bi−Sn system based on experimental data from previous literature and their own work. They defined the thermodynamic parameters $L(0)$ and $L(1)$ for Bi−Sn system to be:

$$L(0) = 500 + 1.5T \tag{C.53}$$

$$L(1) = -100 - 0.135T \tag{C.54}$$

where $L(0)$ and $L(1)$ are given in J/mol, and T is the temperature in K. In this work, these definitions were applied to the sub regular-solution model to calculate the literature values for the vapour pressure of Bi above Bi−Sn alloys at 1173 K, as presented below.

Bi−50 mol% Sn alloy

Ω' and $\frac{d\Omega'}{dx_{Bi}}$ are obtained at 1173 K, for Bi−50 mol% Sn alloy, meaning $x_Bi = 0.5$, as shown in Equation C.55 and Equation C.56.

$$\begin{aligned}\Omega' &= L(0) + L(1)(2x_{Bi} - 1)\\ &= 500 + 1.5(1173) + (-100 - 0.135(1173))(2 \cdot 0.5 - 1)\\ &= 2259.50\end{aligned} \tag{C.55}$$

$$\begin{aligned}\frac{d\Omega'}{dx_{Bi}} &= 2L(1)\\ &= 2(-100 - 0.135(1173))\\ &= -516.71\end{aligned} \tag{C.56}$$

By putting Equation C.55 and C.56 into Equation C.37, and calculating the numerical value, where R is the gas constant in J/Kmol and T is the temperature in K, Equation C.57 is obtained.

$$\begin{aligned}ln\gamma_{Bi} &= \frac{1}{RT}[(1 - x_{Bi})^2\Omega' + x_{Bi}x_{Sn}^2\frac{d\Omega'}{dx_{Bi}}]\\ &= \frac{1}{8.314 \cdot 1173}[(1 - 0.5)^2 \cdot 2259.50 + 0.5 \cdot 0.5^2(-516.71)]\\ &= 0.05129\end{aligned} \tag{C.57}$$

Equation C.57 is solved with respect to γ_{Bi} and the literature partial vapour pressure value calculated as shown in Equation C.58 to C.60.

$$\gamma_{Bi} = exp(0.05129) = 1.05263 \tag{C.58}$$

$$a_{Bi} = x_{Bi}\gamma_{Bi} = 1.05263 \cdot 0.5 = 0.52631 \tag{C.59}$$

$$p_{Bi} = a_{Bi}p^*_{Bi} = 0.52631 \cdot 4.66 \times 10^{-4} = 2.45 \times 10^{-4}\,\text{atm} \tag{C.60}$$

Bi−70 mol% Sn alloy

Ω' and $\frac{d\Omega'}{dx_{Bi}}$ are obtained at 1173 K, for Bi−70 mol% Sn alloy, meaning $x_Bi = 0.3$, as shown in Equation C.61 and Equation C.62.

$$\begin{aligned}\Omega' &= L(0) + L(1)(2x_{Bi} - 1)\\ &= 500 + 1.5(1173) + (-100 - 0.135(1173))(2 \cdot 0.3 - 1)\\ &= 2362.84\end{aligned} \tag{C.61}$$

$$\begin{aligned}\frac{d\Omega'}{dx_{Bi}} &= 2L(1)\\ &= 2(-100 - 0.135(1173))\\ &= -516.71\end{aligned} \tag{C.62}$$

By putting Equation C.61 and C.62 into Equation C.37, and calculating the numerical value, where R is the gas constant in J/Kmol and T is the temperature in K, Equation C.63 is obtained.

$$\begin{aligned}ln\gamma_{Bi} &= \frac{1}{RT}[(1 - x_{Bi})^2\Omega' + x_{Bi}x^2_{Sn}\frac{d\Omega'}{dx_{Bi}}]\\ &= \frac{1}{8.314 \cdot 1173}[(1 - 0.3)^2 \cdot 2362.84 + 0.3 \cdot 0.7^2(-516.71)]\\ &= 0.11093\end{aligned} \tag{C.63}$$

Equation C.63 is solved with respect to γ_{Bi} and the literature partial vapour pressure value as shown through Equation C.64 to C.66.

$$\gamma_{Bi} = exp(0.11093) = 1.11732 \tag{C.64}$$

$$a_{Bi} = x_{Bi}\gamma_{Bi} = 1.11732 \cdot 0.3 = 0.33519 \tag{C.65}$$

$$p_{Bi} = a_{Bi}p^*_{Bi} = 0.33519 \cdot 4.66 \times 10^{-4} = 1.56 \times 10^{-4}\,\text{atm} \tag{C.66}$$

C.3.0.1 Standard error

The standard error was calculated in Excel by use of the function STDEV and SQRT by Equation C.67:

$$Standard\,error = \frac{STDEV(range\,of\,values)}{SQRT(number\,of\,datapoints)} \tag{C.67}$$